STRESS WAVE PROPAGATION IN SPLIT HOPKINSON PRESSURE BAR

Submitted by
Smaranika Nath
(710ce2013)

In partial fulfilment of the requirements
for the award of the degree of

Masters of Technology
in
Civil Engineering
(Structural Engineering)

under the guidance of
Prof. Pradip Sarkar, NIT Rourkela
Dr. Vasant Matsagar (IIT Delhi)

Department of Civil Engineering
National Institute of Technology Rourkela
Orissa -769008, India

NATIONAL INSTITUTE OF TECHNOLOGY
ROURKELA, ORISSA -769008, INDIA

CERTIFICATE

This is to certify that the thesis entitle "**Stress Wave Propagation in Split Hopkinson Pressure Bar**" being submitted by **Smaranika Nath (710ce2013)** in the partial fulfilment of the requirement for the award for the degree of **MASTER OF TECHNOLOGY IN CIVIL ENGINEERING (STRUCTURE)** at the National Institute of Technology, ROURKELA is an authentic work carried out by her under my guidance and supervision. To the best of my knowledge no part of this thesis has been submitted for any other University/Institute for the award of any degree or diploma.

Place: Rourkela, Odisha

Date: 01.06.2015

PROF. PRADIP SARKAR
Associate Professor
Department of Civil Engineering
NIT Rourkela

ACKNOWLEDGEMENTS

This dissertation which I am presenting here can't be completed without the effort of many individuals who has directly and indirectly through their constructive criticism and evaluation, and helped me throughout the year to bring-up this marvelous work of mine to you all. I want to say thanks to all of them from my heart.

First of all, I would like to give my special gratitude to my supervisor **Prof. Pradip Sarkar**, Associate professor, Department of Civil Engineering, NIT Rourkela, for his gracious effort and regular encouragement and support. His dynamism and diligent enthusiasm has been highly instrumental in keeping my spirit high. I am fortunate to have an opportunity to work under him.

I am deeply indebted to **Dr.Vasant Matsagar**, Associate professor, Department of Civil Engineering, Indian Institute of Technology, Delhi, for giving me the opportunity to initiate this project at the Indian Institute of Technology, Delhi. I also thank **Dr.Tanusree Chakraborty,** Assistant professor, Department of Civil Engineering, Indian Institute of Technology, Delhi, for guiding me with my work all throughout the process and taking the pains to patiently deal with my queries and problems, round the clock**.** I am grateful for the support given by the entire faculty and staff of the department.

Finally, I thank to my parents and colleagues for their support and encouragement in the completion of this work.

Smaranika Nath
Roll No. 710ce2013
Rourkela 769008

ABSTRACT

Civil structures are exposed to various impacts due to blast explosion caused by people intentionally or accidentally. Thus buildings in those areas which have threats from explosions should be blast resistant. For this purpose, the dynamic stress-strain responses of various samples of different materials at high strain rates should be found out. The most widely used experimental setup, Split Hopkinson Pressure Bar, has given significant results at high strain rates. It can test the materials at various strain rates in the range of 10 to 10^4/sec.

This apparatus comprises of a short cylinder-like specimen sandwich between two long slender bars. A compressive stress wave is generated by hitting the end of a bar and the wave immediately begins to traverse towards the specimen. The mechanism involved in the apparatus is well explained in the thesis. By tracking the strains in the two bars using different instruments, stress-strain properties of the specimen can be determined.

The intent of this thesis is to study the one dimensional wave propagation on which the SHPB setup is established and to model the one dimensional wave propagation – incidence, reflection and transmission in SIMULINK, a tool in MATLAB. Also, 3D finite element analysis of various types of materials has been done in ABAQUS/Explicit to explore the dynamic behaviour of different types of soft materials which shows plastic properties. The various materials which are modelled and simulated are three types of rocks; limestone, sandstone and granite along with soft materials like cement mortar and concrete.

Key words: high strain rates, compressive stress wave, SIMULINK, ABAQUS, limestone, sandstone, granite mortar and concrete.

CONTENTS

LIST OF FIGURES

Chapter -1

Introduction

1.1. BACKGROUND AND MOTIVATION

In the past few years there is a large increase in fanatic activities of people which can be due to different accidental or intentional events. As a result, civil amenities are witnessing threats from explosive, impulsive loads which are induced due to blast. Fig. 1 shows the damage caused by explosions on civil buildings. Conventional structures are not blast resistant since most designing loads are remarkably lower than that produced during an explosion. These structures are mostly gullible to damage from explosion. Design of blast resistant structures is considered as a specific area that commonly architects and structural engineers are not widely aware of and most of the idea regarding design of blast resistant structures remains limited to defence sectors. This engineering and architectural knowledge can enhance the new and existing buildings to mitigate the effects of an explosion.

Figure 1: Building affected due to blast explosions (Hinman, 2011)

1.1.1. Research Significance

There is sometimes a misunderstanding that the buildings can resist blasts which are designed to resist earthquakes. The structures subjected to blast loading comprise of ground shock, blast pressure and fragment impact specifically in the regions which are quiet near. There are 3 kinds of explosions which are unconfined explosions, confined explosions and explosions caused by

explosives attached to the structure. The resulting shock wave produces in case of nuclear blast are quiet high stresses and large impulsive load turns to destroy the structures even which are at very distant from the source of blast. Due to high explosive blast event the load is applied to the perimeter structural elements of a building, external to the building.

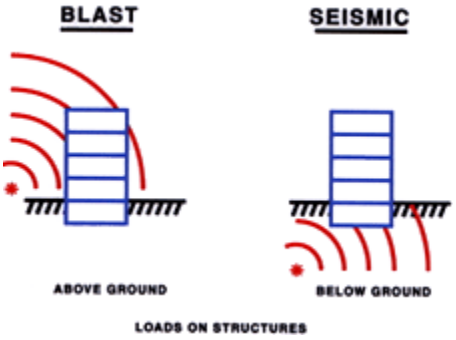

(a) loading type

(b) building responses (c) loading time histories

Figure 2: Comparison between seismic and blast loading (Hinman, 2011).

High intensity in short duration is caused by the pressure wave to the building. The direct effects of an air-blast loading acting on the periphery of a building cannot be met by earthquake resistant buildings. The differences between the loading due to blast and earthquake are as follows:

i. Blast loads act directly on the exterior envelope but as in the case of earthquakes load buildings at the base of the building. (Fig. 2a)

ii. Blast loads normally cause the damage in a localized manner whereas seismic loads cause damage in the global manner. (Fig. 2b)

iii. Blast loads are categorized by a single high pressure impulsive pulse which acts over milliseconds rather than the vibrational loading of earthquakes which acts over seconds. (Fig. 2c)

The behaviour of structures to impact loading has been of much interest to large number of engineers for purposes of designing and also preparing constitutive models for the materials. Blast loadings are of high strain rates which can cause massive damage on the structures. Thus for building blast resistant structures, the engineers should know about the dynamic stress-strain response of various materials. The most widely used apparatus for this purpose is Split Hopkinson Pressure Bar which has given significant results for loadings with high strain rates. The theory that governs the particulars of Hopkinson bar test is spread for many decades.

However, it has only been the past decade, there is a significant data processing improvements in this field. The Split Hopkinson Pressure Bar (SHPB) is a device designed specifically for testing of various materials at strain rates in the range of 10 to 10^4/sec.

1.1.2. Experimental Setup of Split Hopkinson Pressure Bar

Experimental set-up of Split Hopkins Pressure Bar is presented in Fig. 3. The detail of the experimental set-up is as follows:

i. It comprises of three bars striker bar, incident bar and the transmitter bar.

ii. Sample of material is kept between incident and transmitter bar

iii. An uniaxial compressive wave is introduced in the incident bar by shooting the striker bar to the incident bar

iv. The wave propagates to specimen. A part of strain is reflected to incident bar in the form of tension strain wave and rest part is transmitted to the specimen which is again transmitted to the transmitter bar in the form of compressive bar.

v. The strain waves in the input and transmitter bar are monitored by strain gauges attached to those bars.

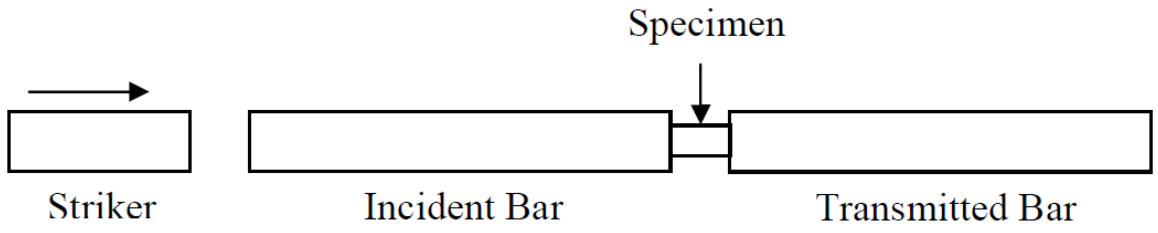

Figure 3: Schematic diagram of Split Hopkinson Pressure Bar apparatus

Few of the assumptions which are considered in this experiment are:

i. The pressures in the bars should remain to a limit which is below the elastic limits so that specimen strain rate, stress and the strain may be determined from the recorded histories of the strain.

ii. Under particular conditions of deformation, two of the strain pulses are need be identified. One is the reflected pulse in the incident bar and the other is the transmitted pulse in the transmission bar.

1.2. OBJECTIVES AND SCOPES

As discussed in the previous section, the analysis of structure subjected to blast loading requires constitutive (stress-strain) relation under high strain rate. There is much literature present the constitutive relation of different civil engineering materials including concrete under high strain rate. Some of these results are based on SHPB experiments and others are based on computer simulation. A detailed literature review reveals that although there are many experiments conducted on concrete in USA and Europe in this regard there are no study reported on the nonlinear stress-strain behaviour using computer simulation. Therefore, the primer objective of the current study is identified as to evaluate the nonlinear stress-strain behaviour of cement mortar and concrete under high strain rate through computer simulation using SIMULINK and ABAQUS. To achieve this main objective the present study has been divided into following sub-objectives:

i) To study the one dimensional wave propagation on which the SHPB setup is established.
ii) To study the methodology involved in obtaining the stress strain data in SHPB.
iii) To validate the methodology using a solved problem from existing literature
iv) To develop nonlinear stress-strain relation of cement mortar and concrete under high strain rate.

1.3. METHODOLOGY

The total work for this project is broken in to parts in order to achieve the proposed objective. Followings are the step by step work methodology defined for this study:

i. Literature Review (Split Hopkinson Pressure Bar, Wave Propagation in bars, dynamic stress-strain responses of different materials)

ii. Model the SHPB setup in graphical programming language tool SIMULINK along with the incidence signal.

iii. Obtain the wave response of incident and transmission bar and finally the stress-strain curve of the specimen.

iv. Model the specimen along with the incident and transmission bar in FE software ABAQUS with appropriate boundary conditions.

v. Obtain the response (stress, strain) of specimen.

vi. Develop constitutive relation for the specimen.

In this study an SHPB setup is modelled using the MATLAB tool, SIMULINK. The properties of the sample is taken and tested with three types of incident waves. Also the wave response of incident and transmission bar is obtained along with the stress-strain curve. Then three types of rocks, i.e., weak sandstone, limestone and granite, are tested under SHPB setup in the finite element software ABAQUS/Explicit 2011. Further brittle materials like mortar and concrete are taken as the sample to find out the dynamic response at different high strain rates. In ABAQUS, there are different types of Plasticity models. In the current study, crushable foam plasticity model is considered for the three rocks while mortar is modelled with the help of Drucker-Prager plasticity model and concrete is modelled in Concrete Damaged plasticity model.

1.4. REPORT ORGANISATION

The thesis is divided into 5 chapters starting with title page, certificate, acknowledgement, table of contents, list of figures and finally references in the last.

Chapter 1 presents the overviews of necessity of studying blast loading. It specifies the difference between earthquake and blasts along with sort description of the experimental setup SHPB used to find out the material's dynamic response under high strain rates.

Chapter 2 presents the chronological development of Hopkinson pressure bar.

Chapter 3 involves the theory and formulations.

Chapter 4 contains the methods followed to find dynamic response of various materials.

Chapter 5 displays the results and discussions.

Chapter 6 contains the summary and conclusion.

Chapter -2

Literature Review

Many other subjects were also reviewed while going through the literature of the split Hopkinson pressure bar. This includes the mechanical properties and materials behaviour of various materials, composite materials etc. It enhances the knowledge about the material science along with engineering involved behind the material behaviour. This chapter includes the sequential progress involved in the building up of the Hopkinson pressure bar. However, some basic idea on how the finite element analysis works for numerical simulation of the whole experiment is as follows.

2.1. FINITE ELEMENT ANALYSIS

FEA is a useful computational method for approximating solutions to a different complex "real-world" engineering problems which have complex domains subjected to general boundary conditions. FEA has turned to be an important step in the design or modelling of a physical phenomenon in different engineering disciplines including civil engineering, aeronautical engineering and many more.

2.1.1. Background

According to Wikipedia, exact date for the origination of the finite element method is very hard to say, but this method serves as the greatest tool to solve the complex and impossible structural analysis problems. Its origination is believed to be the deeds of Hrennikoff (1941) and Courant (1942). In the late 1950s and early 1960s, Feng from China recommended an efficient numerical technique for cracking partial differential equations, based on the computations of dam constructions. This technique was called the finite difference method taking into account an independent invention of finite element method namely the variation principle. In spite of the fact that the methodologies utilized by these pioneers are diverse, they have one essential

characterisation which is the mesh discretization of a continuous domain into a set of separate sub-domains, which are called elements.

The applying of finite element modelling (FEM) has improved dramatically in the recent twenty years with the advent of higher performing computers, advances in modelling software and improved constitutive models. This allows FEM on systems that once seemed nearly impossible to solve. The degradation and failure of a material under extremely high strain rates could only be estimated from dangerous experiments and empirical predictions that are at times impractical and inaccurate. Today, there are numerous fracture and failure models, often pre-loaded in the commercial FEM software. One can simply pick and choose the model that best represents the material system. These models can readily be modified for other material systems and can be translated to many practical applications in industry.

2.2. STRAIN RATE TESTING

Strain rate can be defined as the rate of change of strain with respect to time. Materials behave differently at high strain rates than what at simple static strain rates. Different methods are used to achieve desired strain rates. These methods, such as using conventional load frames for quasi-steady state testing and SHPB for higher strain rates, are chosen to best represent the strain rate and operating conditions of the material with the greatest amount of reproducibility. Table 1 shows some examples of testing methods that are used at various strain rates.

2.3. HOPKINSON PRESSURE BAR PROGRESS

The Split Hopkinson Pressure Bar is an apparatus used to characterize material properties experiencing dynamic loading, which produces high strain and stress waves. In early days,

Hopkinson (1872) performed stress wave experiments to study the behaviour of iron wires (Hopkinson, 1872; Chen and Song, 2011). His experiment included an iron wire held at one end and the other end is free on which a sudden impulse of a mass is loaded. After his works, the yielded results showed the strengthened iron wires under different types of loading.

Table 1: Recommended Testing Methods for Various Strain Rates (Nasser, 2000)

Strain Rate (s^{-1})	Testing Technique
Compression Tests	
<0.1	Conventional Load Frames
0.1-100	Special Servo-hydraulic Frames
0.1-500	Cam Plastometer and Drop Test
200-104	Split Hopkinson Pressure Bar
103-105	Taylor Impact Test
Tension Tests	
<0.1	Conventional Load Frames
0.1-100	Special Servo hydraulic Frames
100-103	Split Hopkinson Pressure Bar (in tension)
104	Expanding Ring
>105	Flyer Plate
Shear and Multi-axial Tests	
<0.1	Conventional Shear Tests
0.1-100	Special Servo hydraulic Frames
10-103	Torsional Impact
100-104	Split Hopkinson Pressure Bar (in torsion)
103-104	Double-notch Shear and Punch
104-107	Pressure-shear Plate Impact

In the findings of Hopkinson (1872) one of the most important was the end of the wire which was fixed would break only with half the speed that would have taken the wire to break at the free end where the mass is loaded (Hopkinson, 1872). His work was succeeded by his son, Hopkinson (1914).

Hopkinson (1914) was the first person to use a bar instead of wire to record an impulsive wave generated by materials after a collision (Chen & Song, 2011). After studying for various years, he concluded that the most important element of collapse of materials was the impact velocity. In his experiments, Hopkinson (1914) had used a pendulum tied to a pencil and used paper to monitor the movements of the rods as the pendulum would hit the desired location as seen in Fig. 4.

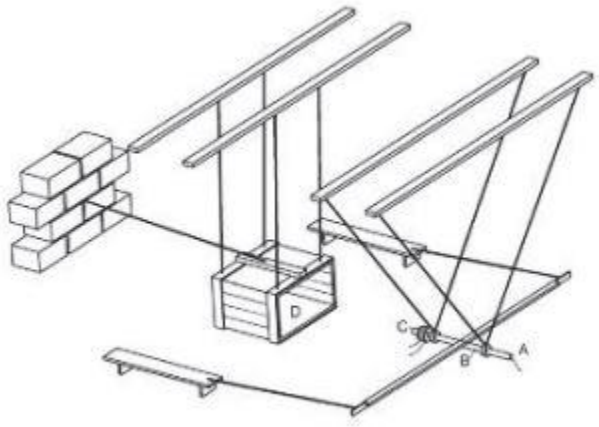

Figure 4: Apparatus for Bertram Hopkinson Experiment (Hopkinson, 1914)

On the other hand, Davies (1948) studied a different technique where he used cylindrical microphones and parallel plates to electrically measure those wave propagations. Davies also mentioned about the propagating and dispersing waves which travel in the long rods. As shown in Fig. 5, Davies' principle benefaction was to improve the HPB mechanism. Davies made various other contributions that can be pointed. He founded that when load is rapidly applied pressures-in the μs scale HPB could not accurately measure them. Also, he found out the time period of creating a pressure wave when an instant force is applied as the wave reaches a

constant value which is related to material's Poisson's ratio. Finally, his last endowment to this field was the discovery of the length-radius relationship of the bar.

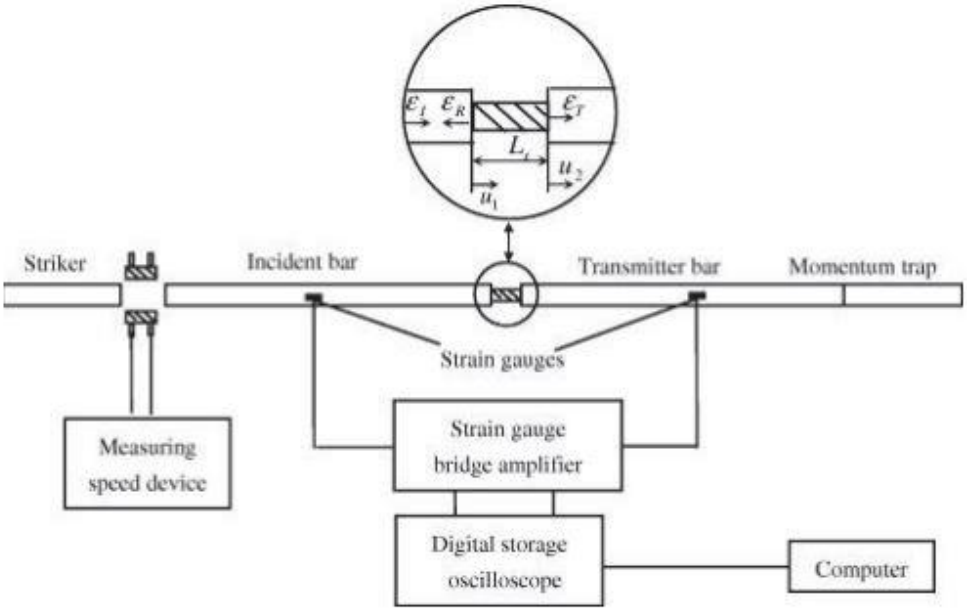

Figure 5: Davies's new improved design of SHPB (Chen, 2010)

While Davies was working on HPB, a modification in that idea has been done by Kolsky in 1949 (Chen & Song, 2011). His work was regarding Hopkinson pressure bar where he modified the original setup by introducing another pressure bar at the end of the testing material specimen. His thought of addition of a second pressure bar at the back of the test specimen allowed him to read the strain data at the back side of the specimen too along with at the front interface. This introduction to the experimental setup succeeded a new vision to the researchers to record not just the strain exerted in the test specimen but also the experienced stress and its strain rate. In his experiments Kolsky also mentioned that by placing specimen in between the input and output bars, the homogenous deformation of the specimen would be allowed. From Davies' work, Kolsky used an electrical condenser for measuring the strains in both input and output bars

which is shown in the Fig. 6. For calculating specimen strain, stress and strain rate he derived equations from the strain data recorded from input as well as output bars. Kolsky's Hopkinson bar setup uses two pressure bars which succeeded and was preferable method for testing materials at high strain rates because of its toughness and accuracy. Since two pressure bars were used by Kolsky unlike Hopkinson who used one pressure bar, the experimental setup was commonly recognized as split Hopkinson pressure bar (SHPB) or Kolsky's bar.

One of the major findings to the HBP was when Krafft et al. (1954) introduced strain gage technology on the yield stress of mild steel with compression to study the effects of static and dynamic loading. After this technology was implemented, various improvements in measuring strain started by 1960. The voltage of a strain gage instrument was measured by the scientists who were able to find relation between the deformation by the changing the resistance of a conductor to the changes in its length and cross sectional area. After the improvisation of the SHPB in 1960's, Hauser et al. (1961) studied the static and dynamic compressive loading of mild steel using strain gages at high temperature. Then many scientists used strain gages in their experiments thus proving that the use of strain gage in the setups has significantly developed the repeatability of the records and also its exactness.

Many scientists improvised the Hopkinson bar experiment by availing high band width signal analysers, high speed computer data acquisition systems, digital storage, which helps in getting much more accurate results with better resolutions. After development of the Hopkinson's experimental setup more researchers tried to study the characterisation of pressure bars, specimen's geometry effects and its numerical modelling. Many of the researchers such as Follansbee and Franz (1983) have put forward dispersion correction methods for eliminating the

oscillations due to stress but their technique is not valid globally for every materials. However, the theory was only effective on small diameter pressure bars.

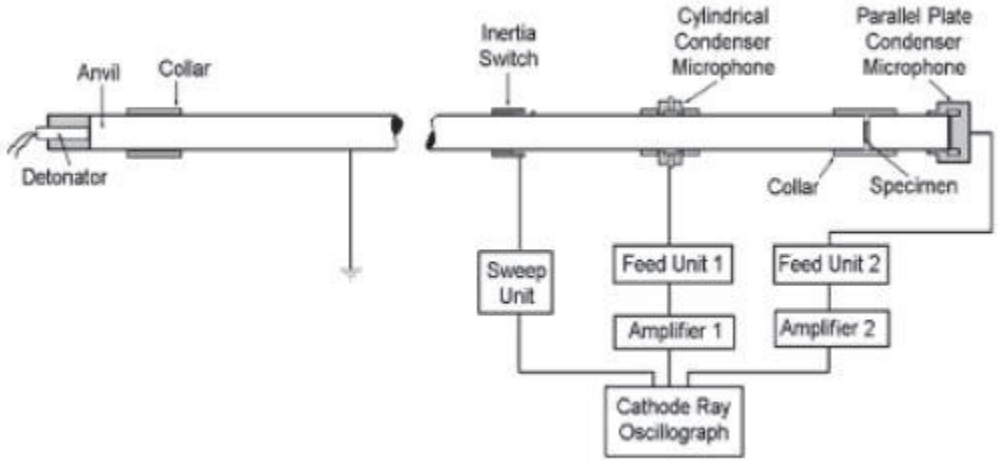

Figure 6: Typical split Hopkinson bar configuration (Chen et al., 2011)

In recent times, the SHPB condemned the use of a parallel plate condenser. It operated using strain gauges attached to both the pressure bars. Those strain gauges are generally attached on the top of the centre of both the bars, which are usually equidistant so that it can help in the acquiring accurate data. The stain gauges direct electrical pulse to a high speed data acquisition system called an oscilloscope. These types of trials can also be monitored with high speed cameras so that an extra visual analysis can be done to get the complete interpretation of the deformation process.

Chapter -3

Theory and Formulation

3.1. WAVE PROPAGATION IN SHPB AND FORMULATION

The SHPB setup consists of two bars, input and output, with a fixed cross-sectional area A_{bar}, modulus of elasticity E_{bar}, and density ρ_{bar}. For developing the governed equation of motion for axial vibration it is only necessary to consider one of them, since the two bars are taken identical. The ratio of length by diameter of the Hopkinson pressure bar is typically taken as 80 or more.

The derivation for the apparatus begins by taking a differential cross section part of a bar before and just after deviation begins. Fig. 7 shows the pressure bar which is non-deformed along with a differential element.

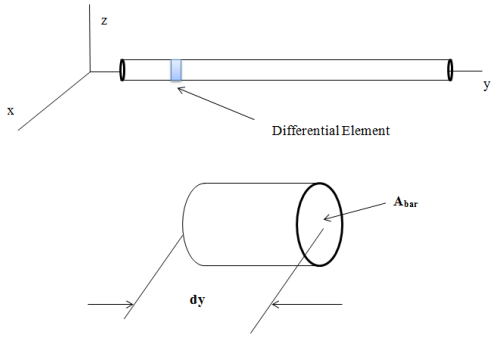

Figure 7: Non-deformed pressure bar shown with its differential element.

The differential element considered has area of cross section A_{bar} and length dy. Before impacting, the bar remains in static equilibrium. As soon as the impact occurs, the differential element's particle experience compression due to forces F_1 and F_2, as shown in Fig. 8.

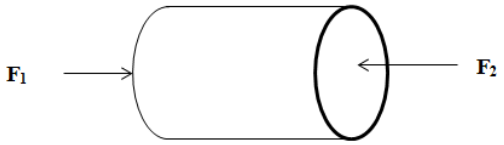

Figure 8: Differential element of bar in compression

In the differential element, the forces that are countering compression are associated to the stresses generated on the cross section of that element. For the elastic bars which obey Hooke's law, there is a relation between stresses and strains by the bar's Young's modulus. However, these strains can be termed with displacements of elements. Therefore, to resist compression, the forces generated can be written in terms of the displacements of elements, *u*, as

$$F_y = A_{bar} E_{bar} \frac{\partial \mathrm{u}}{\partial \mathrm{y}} \tag{1}$$

which is assumed as a uniaxial state of stress. This axial force acting normal to the cross-sectional area of the differential element which is clearly visible in Fig. 9 gives the magnitude of this force.

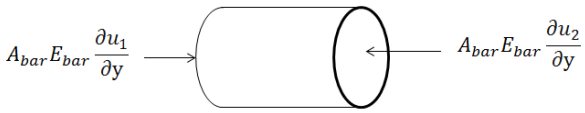

Figure 9: Force resisting compression in differential element

Using Newton's second law, $F=m\,\ddot{y}$, the forces acting on the element are summed up to arrive at the following equation explaining the motion of the pressure waves.

$$A_{bar}E_{bar}\frac{\partial u_2}{\partial \mathrm{y}} - A_{bar}E_{bar}\frac{\partial u_1}{\partial \mathrm{y}} = A_{bar}\mathrm{d}\mathrm{y}\rho\frac{\partial^2 u_1}{\partial t^2} \tag{2}$$

The assumption in this equation is that the acceleration of the particle remains constant throughout the differential element. Clarifying the above equation we get the equation of motion:

$$C_{bar}^2\left[\frac{\partial u_2}{\partial \mathrm{y}} - \frac{\partial u_1}{\partial \mathrm{y}}\right] = \frac{\partial^2 u_1}{\partial t^2}\mathrm{d}\mathrm{y} \tag{3}$$

where C_{bar} is the wave velocity, calculated from

$$C_{bar} = \sqrt{\frac{E_{bar}}{\rho_{bar}}} \tag{4}$$

where E_{bar} and ρ_{bar} are the bars' modulus of elasticity and mass density, respectively. This equation of motion can be simplified by finding relations between the displacements on one side of the differential element to the displacements of the other side which is,

$$u_2 = u_1 + \frac{\partial u_1}{\partial y}\, dy \tag{5}$$

The above equation presumes that the rates of change of displacement of the both the sides of the element are equal, which is obviously reasonable for a differential element. On differentiating, this equation becomes

$$\frac{\partial u_2}{\partial y} = \frac{\partial u_1}{\partial y} + \frac{\partial^2 u_1}{\partial y^2} dy \tag{6}$$

By putting the above equation into (3), the equation of motion for the bar becomes

$$C_{bar}^2 \left[\frac{\partial^2 u_1}{\partial y^2}\right] = \frac{\partial^2 u_1}{\partial t^2} \tag{7}$$

There is no practical use of equation of motion in the analysis of Hopkinson bar, but it gives the theoretical idea of velocity of a wave of undetermined wavelength, which can be used to find out the specimen strain and strain-rate.

3.1.1. Specimen stress

The specimen's average stress can be written in terms of the exerted forces on each of the specimen's surface. A schematic diagram of any cylindrical specimen is shown in Fig.10.

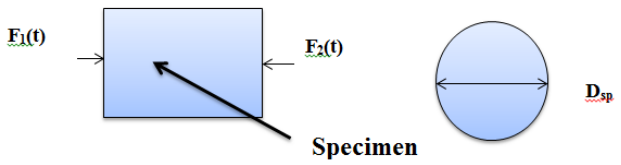

Figure 10: Schematic diagram of the specimen in cylindrical shape

When the specimen is placed in between the pressure bars, forces $F_1(t)$ and $F_2(t)$ exerts on the specimen of diameter D_{sp}. The average force exerted on the specimen is found to be

$$F_{avg}(t) = \frac{F_1(t) + F_2(t)}{2} \tag{8}$$

therefore the average stress on that specimen which is cylindrical in shape is

$$\sigma_{avg}(t) = \frac{F_{avg}(t)}{\frac{\pi {D_{sp}}^2}{4}} \tag{9}$$

The forces $F_1(t)$ and $F_2(t)$ which are exerting at the specimen surfaces is caused by the pressure bars. The forces at the cross-sectional ends of the pressure bars for a specimen in dynamic equilibrium can be coined in terms of the both incident and reflected strains of the pressure bars as

$$F_1(t) = (E_{bar}\,[\varepsilon_i\,(t) + \varepsilon_r\,(t)])\frac{\pi {D_{bar}}^2}{4} \tag{10}$$

$$F_2(t) = (E_{bar}\varepsilon_t\,(t))\frac{\pi {D_{bar}}^2}{4} \tag{11}$$

where D_{bar} is the pressure bars' diameter. Replacing equations (8),(10) and (11) into equation (9) we get the average stress on the specimen in terms of the strain generated in pressure bars

$$\sigma_{avg}(t) = \frac{{D_{bar}}^2}{2{D_{sp}}^2} E_{bar}[\varepsilon_i(t) + \varepsilon_r(t) + \varepsilon_t(t)] \tag{12}$$

If there is a uniform deformation of specimen as assumed, the strains generated in the incident bar can be equated to the strain generated in the transmission bar

$$\varepsilon_i(t) + \varepsilon_r(t) = \varepsilon_t(t) \tag{13}$$

Thus the average stress in a specimen can be portrayed as

$$\sigma_{avg}(t) = \frac{{D_{bar}}^2}{{D_{sp}}^2} E_{bar}\varepsilon_t(t) \tag{14}$$

This equation clearly mentions that the stress on the specimen is proportional to the amplitude of the strain transmitted into the transmitter bar through the specimen.

3.1.2. Specimen strain rate and strain

The average strain rate can be defined as the average strain by the time until which the strain in a body continues. Strain implies deformation i.e. displacement, which when divided by time gives velocity. From the velocities at the interfaces of pressure bar – specimen the specimen strain rate can be found out. The strains generated in the pressure bars helps to calculate the interface velocities. The derivation of the expressions for the specimen's strain rate and strain in terms of the pressure bars' strains, the pressure bars' equation of motion is recalled which is shown here for convenience.

Considering the displacement of the bar of incidence as u_1 and the bar of transmission as u_2, it can be written as

$$u_1 = \int_0^t C_{bar}\, \varepsilon_1(t) dt \tag{15}$$

And

$$u_2 = \int_0^t C_{bar}\, \varepsilon_2(t) dt \tag{16}$$

where the subscripts 1 and 2 are referred, respectively, to the left and right end of the specimen. Equations (15) and (16) can be rewritten as a function of the incident, reflected and transmitted pulses:

$$u_1 = C_{bar} \int_0^t (\varepsilon_i - \varepsilon_r) dt \tag{17}$$

And

$$u_2 = C_{bar} \int_0^t \varepsilon_t\, dt \tag{18}$$

The compressive stresses and strains are considered positive. As assumed, the uniformity in the state of strain and stress in the specimen thickness, its strain, ε_s, is given by the expression below:

$$\varepsilon_s = \frac{u_1 - u_2}{L_{sp}} \tag{19}$$

where L_{sp} represents the specimen length. Substituting Eq. (17) and (18) into Eq. (19) the strain the specimen is subject to is given by:

$$\varepsilon_s(t) = \frac{C_{bar}}{L_{sp}} \int_0^t (\varepsilon_i - \varepsilon_r - \varepsilon_t) dt \tag{20}$$

From equation (13), equation (20) can be written as

$$\varepsilon_s(t) = -\frac{2C_{bar}}{L_{sp}} \int_0^t \varepsilon_r \, dt \tag{21}$$

Also the strain rate is given by,

$$\dot{\varepsilon} = \frac{2C_{bar}\varepsilon_r}{L_{bar}} \tag{22}$$

Once the equilibrium of force is established, equations (13), (14), (21) and (22) are valid immediately. When the specimen deforms by just crossing the yield point of the material used as specimen, from one dimensional Hooke's law the following relationship is satisfied:

$$\sigma_y = E_{bar}\varepsilon_y \tag{23}$$

where σ_y and E_{sp} are the yield stress and modulus of elasticity of the specimen respectively.

3.2. MODELLING AND SIMULATION IN SIMULINK

The split Hopkinson pressure bar can be modelled and simulated using the MATLAB toolbox SIMULINK. It follows some fundamental concepts while modelling. Finally the stress strain curve is found out after simulation in the software.

3.2.1. Fundamentals of 1D stress wave propagation

1-D stress wave's basic behaviour-

When a compressive stress wave strikes an interface between two different material part of the incident wave transmit from one material to other and part of it gets reflected in the same

material. Basically, the behaviours of one dimensional elastic stress wave consist of transmission, reflection and linear superposition. Transmission and reflection occur at the interface of bar-specimen when a stress wave propagates with different generalized mechanical impedance. When a stress wave starts propagating from bar 1 to bar 2, the general mechanical impedances of both bars are $(\rho CA)_1$ and $(\rho CA)_2$, respectively, and the relation between the area of the cross-sectional of 1 and 2 along with the relation of impedance of 1 and 2 are denoted as

$$\alpha = \frac{A_1}{A_2}$$

$$\beta = \frac{(\rho CA)_1}{(\rho CA)_2} \tag{24}$$

And the transmission and reflection coefficients can be expressed as

$$T_{12} = \frac{2\alpha}{1+\beta}$$

$$R_{12} = \frac{1-\beta}{1+\beta} \tag{25}$$

respectively. Therefore, if the stress pulse incidence is considered as σ_i, the transmitted and reflected waves can be depicted as $T_{12}\,\sigma_i$ and $R_{12}\,\sigma_i$ respectively.

Furthermore, the principle of superposition can be avail in the one dimensional elastic stress wave. That implies the overall stress at a particular point is the linear superposition of all the amplitudes of stress waves that are propagating.

The stress wave reflects and transmits as back and forth many a times in the specimen until equilibrium is achieved. The strain wave which gets reflected (ε_r) equates to the summation of all the left sided strain waves generated in the input bar and the strain wave which gets transmitted (ε_t) equates to the summation of all the right sided strain waves generated in the output bar.

The Foundation of SHPB shown in Fig. 11:

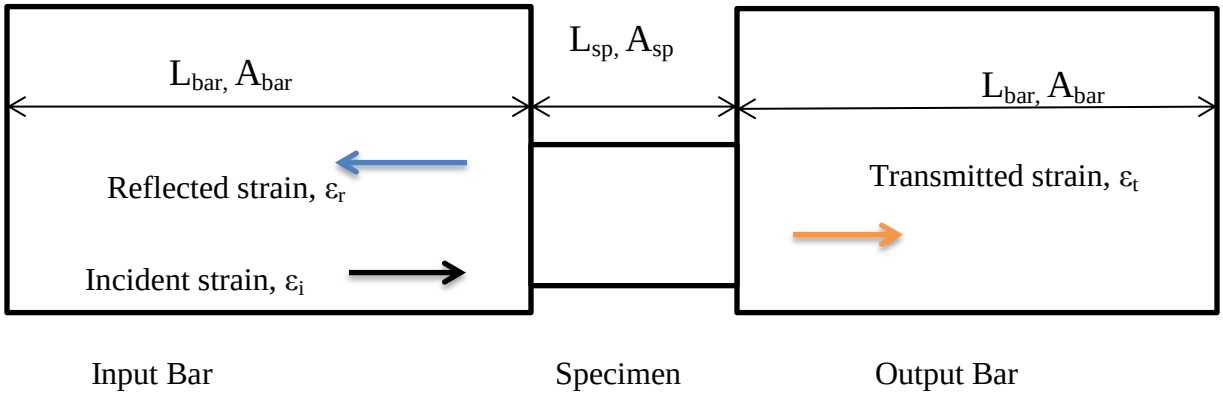

Figure 11: Foundation of SHPB

The propagation of stress wave in an SHPB test is shown in Fig. 12:

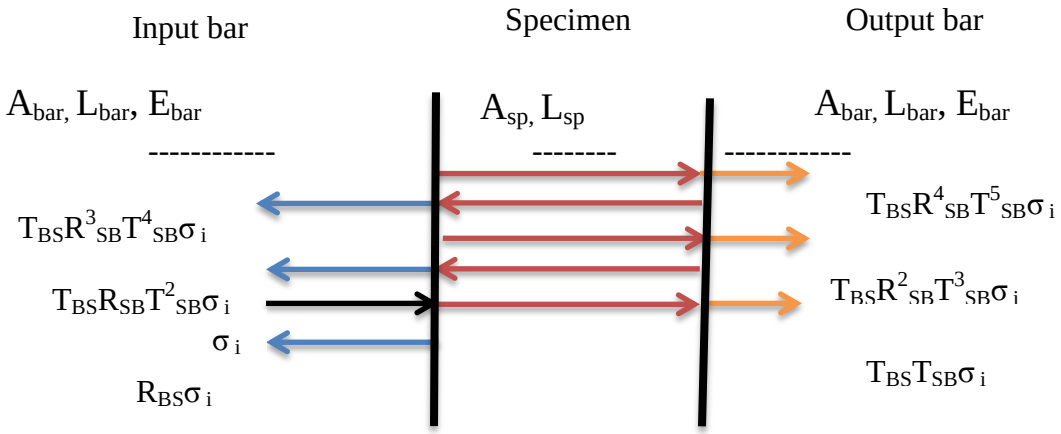

Figure 12: Propagation of stress wave in SHPB test

3.2.2. Incidence of the Striker

In the test using the SHPB setup striker bar is used to produce impact on the end of the cross-section of the input bar. As the striker collides with the cross-sectional end of bar of incidence in the axial direction with *V* as an initial velocity, an incident stress impulse in the form of trapezoid is generated which propagates down the incident bar. The intensity of stress generated on the bar

is given as:

$$\sigma_i = \frac{1}{2}(\rho_{bar} C_{bar} V) \quad (26)$$

while the time period of the stress impulse created is given as:

$$\Delta t = 2\frac{L_s}{C_{bar}} \quad (27)$$

Where V is the striker's velocity; L_S is striker's length.

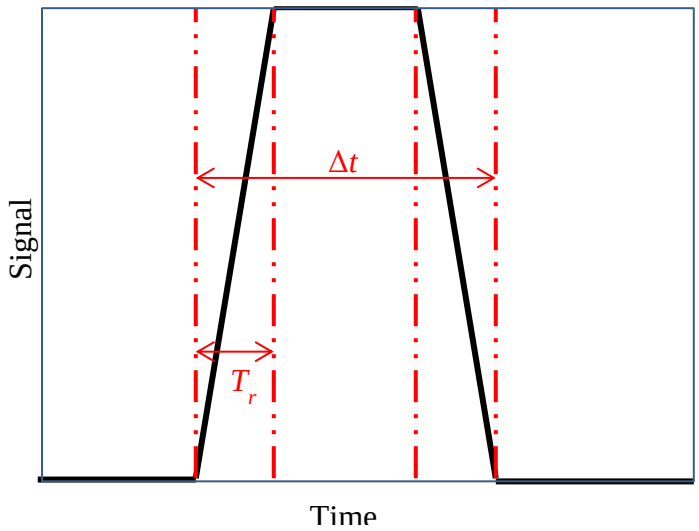

Figure 13: A trapezoidal signal with Tr as the rising time and Δt as time duration

The elastic stress pulse generated then propagates along the bar of incidence with an axial elastic wave velocity. The method of loading which can generate a trapezoidal incident pulse by a striker has been proved to be reliable up to some extent (Li et al., 2006) which is shown in the Fig. 13.

3.3. NUMERICAL ANALYSIS FOR ROCKS

To understand the impact induced stress-strain response of rocks up to 100/sec strain rate through numerical simulation of uniaxial SHPB tests on different types of rocks have been done. Numerical simulations which have been increasingly used in the designs used by engineers

require an exact family of stress-strain curves at various strain rates to obtain the impact responses. Reliable dynamic experiments on soft materials like rocks must be designed and carried out to determine such dynamic stress-strain curves before a strain-rate-dependent material model can be developed. Although it is a reliable method due to its efficiency inside the laboratory, there are some crucial mechanisms like propagation of wave, the process of failure in the specimen, stress interference and effect of the strain rate, which are important for explaining the system performance and specimen behaviours which are still unclear because of the restrictions in the present testing methods. High strain rate material constitutive models have been used to characterize the rock sample.

The SHPB test has been helpful to find out the dynamic compressive and tensile strength of rocks. The dynamic increase factor (DIF) for rocks, which is defined as the ratio of the dynamic uniaxial compressive strength to the quasi-static uniaxial compressive strength, gradually increases with strain rate when the strain rate is at its lower regime (10^{-4}-10^{1}/sec), however there is a rapid increase in the intermediate (10^{1}-10^{2}/sec) as well as high (10^{2}-10^{4}/sec) strain rate regimes. As compare to quasi-static experiments, dynamic characterization of materials, especially rocks, at high strain rates is still much more challenging since currently-available dynamic testing techniques have been less capable of obtaining reliable stress-strain data at high strain rates.

3.3.1. Characters of rocks and brittle materials

The ultimate dynamic stress-strain response curves obtained by SHPB tests on rocks and brittle materials which are compared with metallic materials may be credited to the following factors:

- Due to *the heterogeneity of rocks*, the pressure bars' diameter in an SHPB used for rock and other brittle materials should not be too small or too large.

- Due to *material brittleness*, the disturbance in the incident stress pulse may cause serious violation of both the transmitted and reflected waves. Therefore, the length to diameter ratio of the specimen should not be too small. It is usually considered larger than 0.5. The specimen force is the average force at the two ends of the specimen.
- Due to *the strength of rock materials*, the modulus of elasticity is comparatively low than the metals.

3.3.2. Numerical Analysis using ABAQUS

The finite element (FE) software ABAQUS has been used with explicit time integration scheme to simulate the SHPB tests on rocks. Characterization of rock behaviour under impact loading for strain rates of wide ranges requires both experimental and numerical simulation of SHPB tests on rock under uniaxial conditions. It is important to study the numerical simulation of SHPB tests on rocks considering the elasto-plastic behaviour of rocks. The schematic diagram of the SHPB setup is shown in Fig. 14.

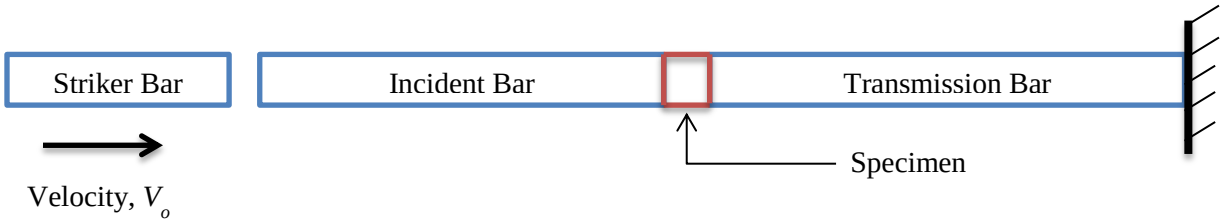

Figure 14: The schematic model of SHPB setup

3.3.3. Crushable Foam Plasticity Model

The constitutive models of crushable foams typically used in structures which absorb energy and are available in ABAQUS for the analysis. Two constitutive models are presented: the volumetric hardening model and the isotropic hardening model. The volumetric hardening of the

model is defined by providing the experimental data for uniaxial compressive strength with axial strain. The isotropic hardening model was originated by Deshpande and Fleck (2000) for metallic foams. Symmetric behaviour in tension and compression was assumed, and an equivalent plastic strain governs the evolution of the yield surface, which has contributions from both the deviatoric plastic strain and the volumetric plastic strain. The mechanical behaviour of crushable foams is known to be sensitive to the straining rate. This effect introduces a piecewise linear law or by the overstress power law model. The elastic behaviour can be modelled only as linear elastic.

$$\sigma = D^{el}\varepsilon^{el} \tag{28}$$

where D^{el}represents the fourth-order elasticity tensor and σ and ε^{el} are the second-order stress and elastic strain tensors, respectively.

The crushable foam plasticity constitutive model can simulate compressive stress induced compaction behaviour. The yield surface of the model takes an elliptical shape in the mean stress (p) vs. deviatoric stress (q) plane. Inside the yield surface, the behaviour of the rocks remains linear elastic. The elliptical yield surface equation of the model is given by

$$F = \sqrt{q^2 + \alpha^2(p - p_0)^2} - B = 0 \tag{29}$$

where p_0 is given by $(p_c - p_t)/2$; $p_c$and $p_t$are the yield strength values of the rocks under hydrostatic compression and tension, respectively. The parameter B is the magnitude of the intercept of the yield surface with the vertical axis for deviatoric stress q; and the parameter α define the yield surface's shape in the meridional plane.

For the isotropic hardening model the flow potential is chosen as

$$G = \sqrt{q^2 + \beta^2 p^2} \tag{30}$$

where β represents the flow potential's shape in the p–q stress plane which is related to the plastic Poisson's ratio, ν_p, by

$$\beta = \frac{3}{\sqrt{2}}\sqrt{\frac{1-2\nu_p}{1+\nu_p}} \tag{31}$$

The plastic Poisson's ratio can be defined as the ratio of the transverse plastic strain to the longitudinal plastic strain under uniaxial compression. It must be between –1 and 0.5. The upper limit, $\nu_p = 0.5$, corresponds to an incompressible plastic flow. The plastic strains are defined to be normal to a family of self-similar flow potentials parameterized by the value of the potential *G*.

3.4. NUMERICAL ANALYSIS FOR MORTAR:

It is necessary to analyse the effect of strain rate on strength of various materials e.g., concrete, mortar and geo-materials, since it is one of the important factor for modelling and designing of structures experiencing high strain rate when subjected to impacts or explosive loading. The SHPB test has been used to determine the dynamic compressive and tensile strength of mortar.

It is generally accepted that when the concrete-like material is treated with high strain-rate there is an apparent rise in the dynamic strength. Due to its broad applications in impact and blast loading environment, the dynamic strength enhancement of concrete has drag attentions of engineers in the field of structural design and analysis. A very important factor is the lateral confinement in a SHPB test which may cause the enhancement of dynamic strength of concrete by increasing the strain-rate. The lateral confinement comes from both the lateral inertia and the contact surface restriction during the rapid compression.

3.4.1. Drucker–Prager plasticity model

Drucker and Prager (1952) proposed this DP model. It can well describe for pressure-sensitive materials such mortar and concrete. DP model is provides a phenomenological account due to the internal friction for the pressure dependent flow which is a typical feature of concrete or concrete-like materials. It allows the evolution of the deformation to be tracked through both the strain softening and the strain hardening within the framework of definite deformation kinematics. In the case of uniaxial compression with uniform confinement the details of the model are described briefly in the following sections.

Yielding criterion and softening/hardening rule

The criterion of linear Drucker-Prager is written as

$$\mathrm{F} = t - p\tan\beta - d = 0 \tag{32}$$

Where, t is the deviatoric stress measured and defined as

$$\mathrm{t} = \frac{1}{2} q \left[1 + \frac{1}{K} - \left(1 - \frac{1}{K}\right)\left(\frac{r}{q}\right)^3\right] \tag{33}$$

β is the linear yield surface's slope in the *p–t* stress plane. It is mostly referred to as the angle of friction of the material where *d* is the cohesion of the material and K is called the stress flow ratio. Stress Flow ratio is defined as the ratio of the yield stress in tension to the yield stress in compression in a triaxial test, which controls the dependence of the yield surface on the value of the intermediate principal stress.

Plastic flow

In this model *G* is the flow potential chosen as

$$G = t - p\tan\psi \quad (33)$$

where ψ is the angle of dilation in the *p*–*t* plane.

3.5. NUMERICAL ANALYSIS OF CONCRETE

Solid structures regularly confront high rate dynamic loadings, for example, tremor, sways, blasts, and so forth. Thus, it is important to know the properties of solid materials so as to anticipate the reaction of the solid structure under such dynamic of loading. The mechanical properties of concrete based materials are sensitive to strain rate. The fundamental properties of concrete; Specifically, viscoelasticity of solidify concrete and crack enlargement. The property of consistency relies on upon rate of strain and free water present in the materials of cement (Rossi et al., 1992). This study had demonstrated that the rate impact of cement is influenced by two factors; the free water viscosity dominating under lower loading rate and the inertia effect under higher strain rate. The dynamic conduct especially stretch strain conduct of NSC example was mulled over by utilizing programming ABAQUS/Explicit under high strain rate.

3.5.1. Concrete damaged plasticity model

The concrete damaged plasticity has the potential of representing complete inelastic characteristics of concrete both in tension as well as compression including damage characteristics. It model presumes that the two main mechanisms of failure in concrete are cracking due to tension and crushing due to compression. In this model, uniaxial compressive behaviour and tensile is considered as damaged plasticity.

The material model is a continuum, plasticity based, damaged model for concrete. Damaged plasticity is assumed to characterize the uniaxial compressive and tensile response of concrete as shown in Figure 15. At the beginning, the stress-strain relationship is linearly elastic under

uniaxial tension until the stress at which failure occur f_{t0} is reached. Failure stresses in concrete block is converted to replace microcracks in it. Beyond the state of the failure stress in concrete, stress-strain response is designed by softening characteristic (Fig. 15a).

In uniaxial compression, the behaviour is linear until the initial yield stress f_{c0}. After attaining the ultimate stress f_{cu} in the plastic zone, the response of concrete is characterized by the stress hardening which is then succeeded by strain softening (Fig. 15b). Therefore, concrete stresses determined unloading from any point on the strain are

$$f_t = E_c(\varepsilon_t - {\varepsilon_t}^{pl})(1 - d_t)$$

$$f_c = E_c(\varepsilon_c - {\varepsilon_c}^{pl})(1 - d_c) \quad (34)$$

where E_c is the modulus of elasticity of concrete. Then, the effective tensile and compressive cohesion stresses of concrete are estimated as

$$\overline{f_t} = \frac{f_t}{(1-d_t)} = E_c(\varepsilon_t - {\varepsilon_t}^{pl})$$

$$\overline{f_c} = \frac{f_c}{(1-d_c)} = E_c(\varepsilon_c - {\varepsilon_c}^{pl}) \quad (35)$$

which determine the size of the failure surface. The post failure behaviour of reinforced concrete represents by means of the post failure stress as a function of cracking strain ${\varepsilon_t}^{ck}$ and ${\varepsilon_c}^{ck}$, which can be defined as the subtraction of the elastic strain from the total strain corresponding to the undamaged material, and the data for tension stiffening are given in terms of the cracking strains. When unloading data are available, programming automatically converts the cracking strain values to plastic strain values using the following relationships (ABAQUS/Explicit):

$$\varepsilon_t{}^{pl} = \varepsilon_t{}^{ck} - \frac{d_t}{(1-d_t)}\frac{f_t}{E_0}$$

$$\varepsilon_c{}^{pl} = \varepsilon_c{}^{ck} - \frac{d_c}{(1-d_c)}\frac{f_c}{E_0} \quad (36)$$

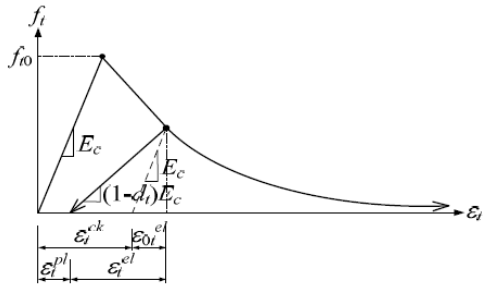

(a) Tension behaviour associated with tension stiffening

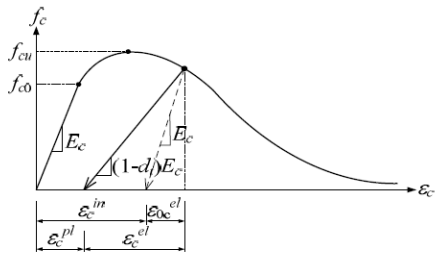

(b) Compressive behaviour associated with compression hardening

Figure 15: Concrete damaged plasticity model (Ali, 2014)

Chapter -4

Methodology and Present Work

4.1. MODELLING AND SIMULATION

When the incident pulse reaches at one interface, it can be divided into two different signals (which are equal to source pulse). From there, they enter into two different Gain blocks (which are usually called amplifiers), Gain 1 and Gain 2, with different coefficients for reflection and transmission, respectively. The Fig. 16 gives the stress propagation at one of the interface.

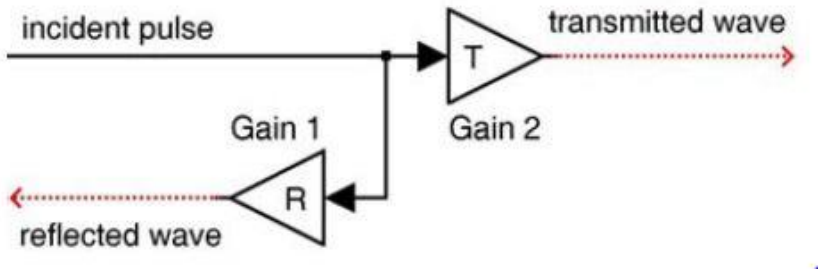

Figure 16: Transmission and reflection of stress wave propagation at interface

Two stress waves can be linearly superimposed as shown in Fig. 17. Here, the two stress waves (stress wave 1 and stress wave 2) directly pass to a Sum block and therefore their linear superposition (stress wave 3) is comes as an output.

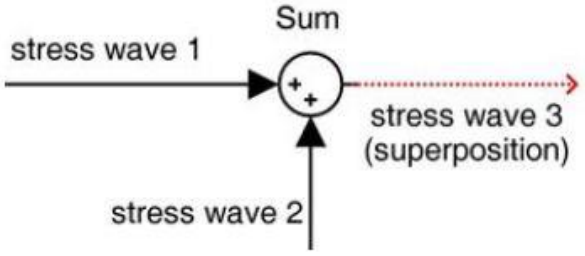

Figure 17: Linear superposition of stress wave

The back and forth reflection and transmission of stress wave in SHPB test is shown in the Fig. 18 below. Here a loop is formed and the stress waves keep getting superimposed. Finally the reflected stress waves and transmitted waves are generated.

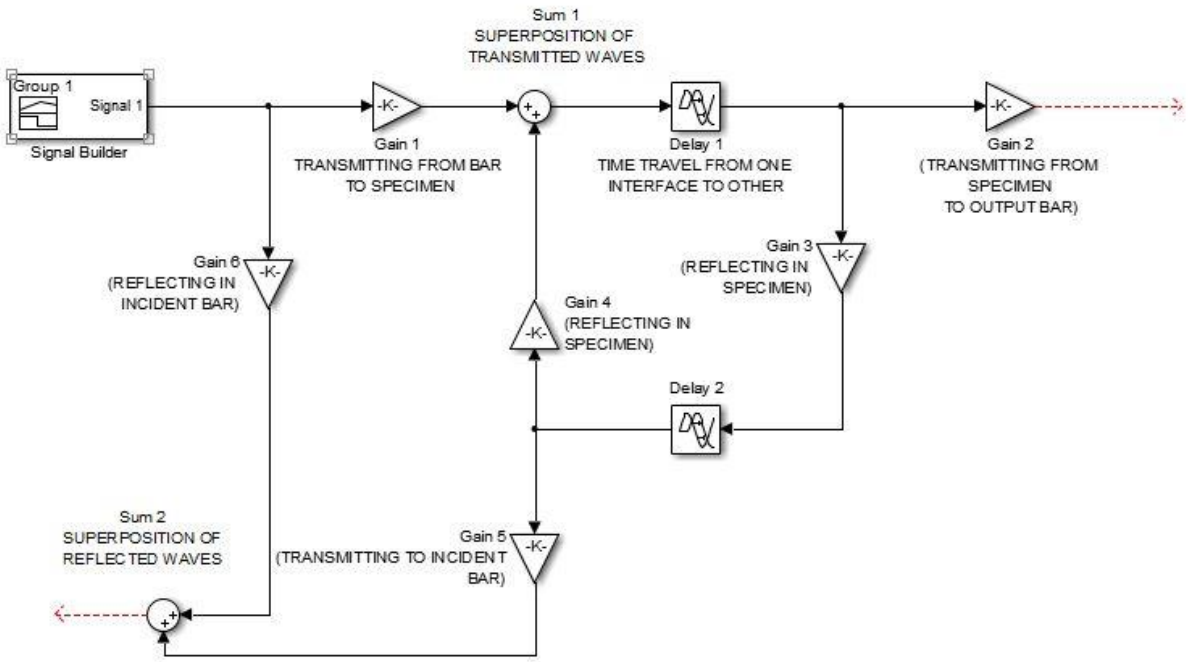

Figure 18: Back and forth of reflection and transmission wave in SHPB test

4.1.1. Split Hopkinson Pressure Bar modelling in SIMULINK

The basic phenomenon of modelling and simulation are discussed above. The stress wave transmits and reflects until the homogenization occurs in the SHPB test. Here to simulate the back-and-forth reflections and transmissions a feedback loop technique is utilized. The Fig. 19 shows the complete modelling of the SHPB setup. In this the incident pulse propagates to the bar-specimen interface where a fraction of it gets transmitted while a fraction of it gets reflected. The Gain1 block is used to obtain transmitted wave. The Delay block 1 is used to delay the stress wave by the time it travels inside the specimen from one interface to the other. Here transmission

occurs at the specimen-bar interface using the Gain2 block. Gain7 block is used to generate the final stress which is the product of a constant with the total transmitted wave. Gain6 is the reflected coefficient at the first interface i.e., the when the signal was propagating from bar to specimen while Gain3 block is the reflected coefficient at the second interface i.e., the specimen-bar interface. Delay2 is followed by the Gain3 block which is the time delayed due to the back propagating of the stress wave from second interface to the first interface. Again at the interface there is a Gain4 block which obtains reflected wave at the first interface. This signal gets superimposed with the transmitted signal obtained by the Gain1 block. This is obtained by using Sum1 block. There a loop is created. The Gain5 block is used to obtain the transmitted wave of the back propagating wave at the first interface. This wave gets superimposed with the reflected wave obtained by Gain6 block. Here Sum2 block is used. Then, all the above blocks together forms a feedback loop. The signals of the total transmission and reflection can be extracted in the looping process. Finally according to the above formula and integrator is used to integrate the superimposed reflected signal propagating backwardly which is then multiplied with a constant for which Gain8 block is used. The strain in the specimen is found out. At the end the graph between the stress and strain is found using the XY Graph block.

According to Yongjian et al, (2010), three types of incident waves are taken: rectangular, finite rising and sloping and its stress-strain responses are found using the XY Graph block. The variables, such as the transmission and reflection coefficients, before running this model need to be valued and saved in the workspace of MATLAB SIMULINK by insertion or calculation. The parameters required for the SHPB configuration were set as:

Young's Modulus of incident and transmission bar, E_{bar} = 200E9 Pa,

Young's Modulus of the specimen, E_{sp} = 200E9 Pa,

Wave velocity, $C_{bar} = C_{sp}$ = 5064 m/s,

Length of Specimen, L_{sp} = 5.064E-3 m,

Bar Impedance Ratios for bar-specimen interface, α = ß = 10

Bar Impedance Ratios for specimen-bar interface, α = ß = 1/10

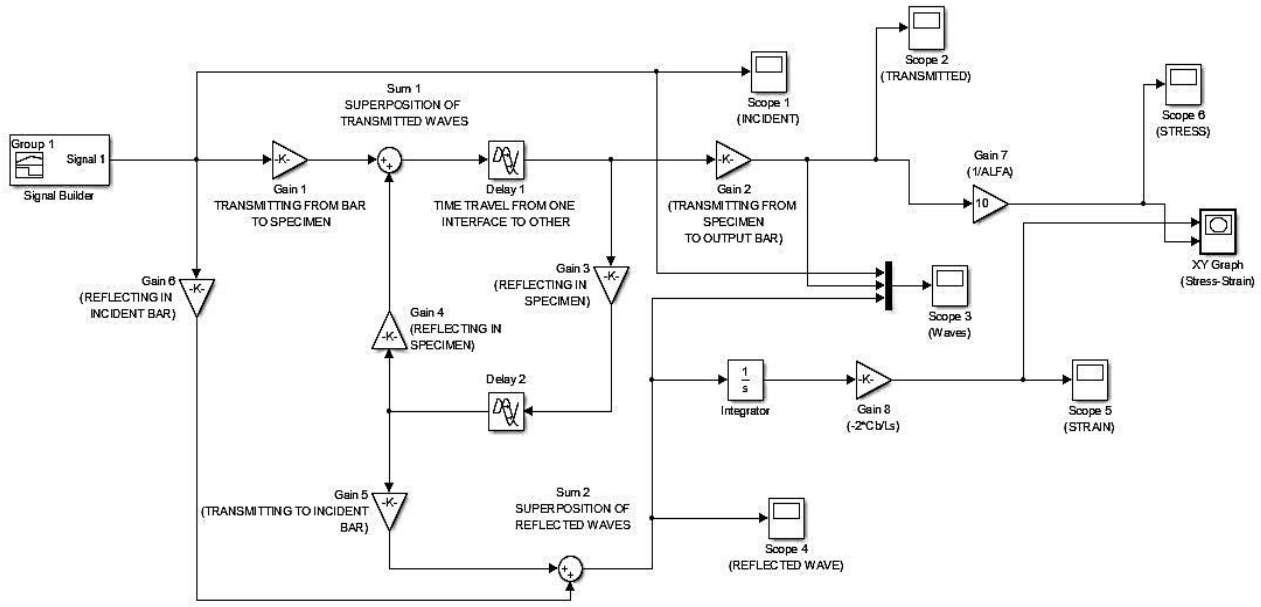

Figure 19: Simulation model of the SHPB configuration

4.2. MODELLING AND SIMULATION IN ABAQUS

A finite element (FE) analysis technique using ABAQUS is chosen to explore the dynamic behaviour of different types of soft materials which shows plastic properties. FE analyses were performed implementing ABAQUS/Explicit 6.11 programming tool to predict the dynamic responses under the pressure amplitude introduced by a striker bar on the surface of incident bar. There are some basic steps followed as shown in the flow chart in Fig. 20.

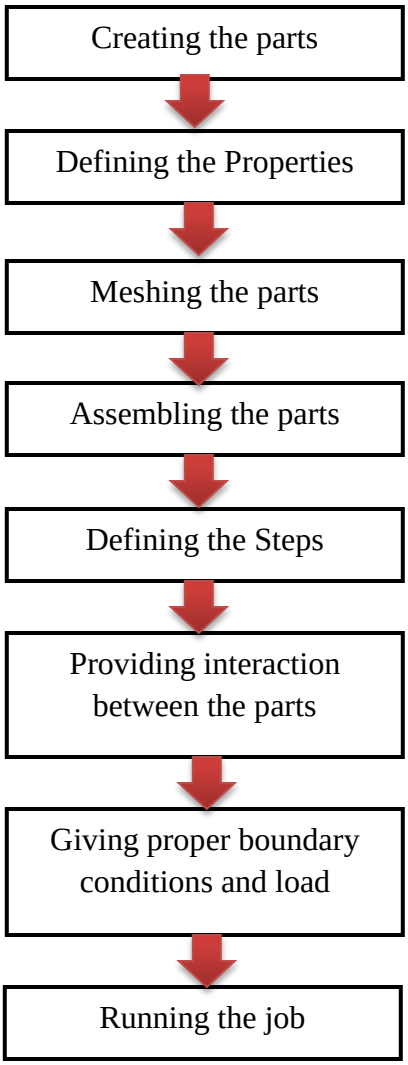

Figure 20: Basic steps followed in ABAQUS

4.2.1. Modelling and simulating three types of rocks

Before the numerical simulation of the three types of rocks, the properties of bars and samples are found out. A 3D model of the SHPB setup is used for analysing and simulating purpose.

Modelling the parts and their properties

- The incident, transmitted and striker bar are taken as High strength maraging VM350 steel. Three dimensional model of these individual bars and the specimen are presented in Fig. 21. The properties of the materials are given in Table 2.

- Three rock samples, limestone, sandstone and granite are taken to be tested in SHPB setup. The diameter and length of sample considered is 12.7 mm.
- The properties of the materials are given in Table 3.

Table 2: Properties of bars

Bars	Diameter (mm)	Length (m)	Mass Density, ρ (kg/m^3)	Modulus of elasticity, E (GPa)	Poisson Ratio, ν
Striker bar	12.7	0.152	8100	200	0.3
Incident bar	12.7	2.13	8100	200	0.3
Transmit bar	12.7	.915	8100	200	0.3

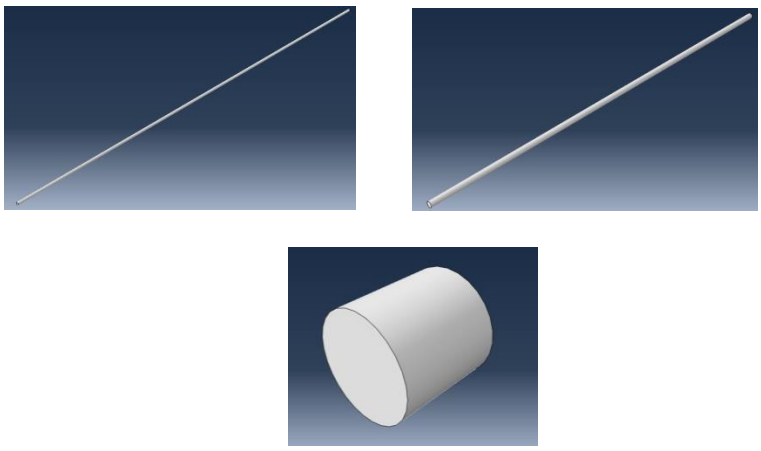

Figure 21: The incident bar, transmit bar and the specimen in ABAQUS window

Table 3: Properties of rocks

Rock type	Mass Density, ρ (kg/m^3)	Modulus of elasticity, E (GPa)	Poisson Ratio, ν	Yield strength, σ_y (MPa)
Limestone	2300	24	0.35	68
Weak Sandstone	2291	4.86	0.35	23
Granite	2620	50	0.17	200

- In the present investigation, the crushable foam plasticity model in ABAQUS has been used to model soft rocks, e.g., limestone and weak sandstone. The performance of the model has also been tested for hard rock, e.g., granite.
- The stress-strain curves for the limestone, weak sandstone and granite are obtained from the graphs as shown in Fig. 22 and used as input in ABAQUS.

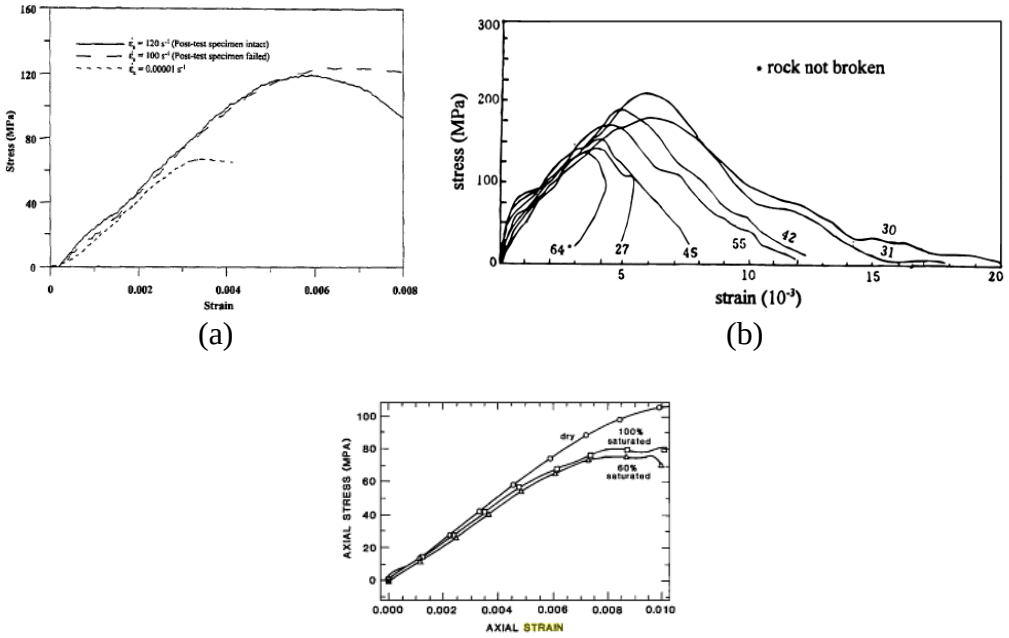

(a) (b)

(c)

Figure 22: The stress-strain curves for (a) limestone (Yang, 2005), (b) granite (Li et al., 2006) and (c) weak sandstone (Duba et al., 2010).

- The strain rate dependence of rocks is included in the model by defining the increase of dynamic yield strength with respect to the static yield strength, i.e., the dynamic increase factor (DIF) with the increase in strain rate. Table 4 shows the DIF of different samples with increase in strain rates.

Table 4: Dynamic increase factor (DIF) for different materials (Chakraborty, 2013).

Sl no.	Material	Strain rate (ε) /sec	Dynamic Increase Factor (DIF)
1	Limestone	0	1
		0.01	1.36
		0.1	1.47
		1	1.59
		10	1.71
		100	1.83
		1000	1.95
2	Weak Sandstone	0	1
		0.01	1.4
		0.1	1.85
		1	2.5
		10	3.2
		100	4.27
		1000	5.63
3	Granite	0	1
		1	1.36
		5	1.4
		45	1.45
		145	1.59
		676	1.9
		731	2.15
		1023	2.27
		2344	2.47

Creating Mesh:

- Three dimensional (3D) solid eight node brick elements with reduced integration and hourglass control (C3D8R) are used for meshing the incident bar, transmission bar and the rock sample. The large mesh distortion is taken into account under C3D8R elements without hampering the results as it consider volumetric locking which is a usual problem in analysis of large deformation.
- The incident bar is meshed to 83070 elements, while the sample was meshed to 17250 elements and there are 33123 elements in transmitted bar as shown in Fig. 23.

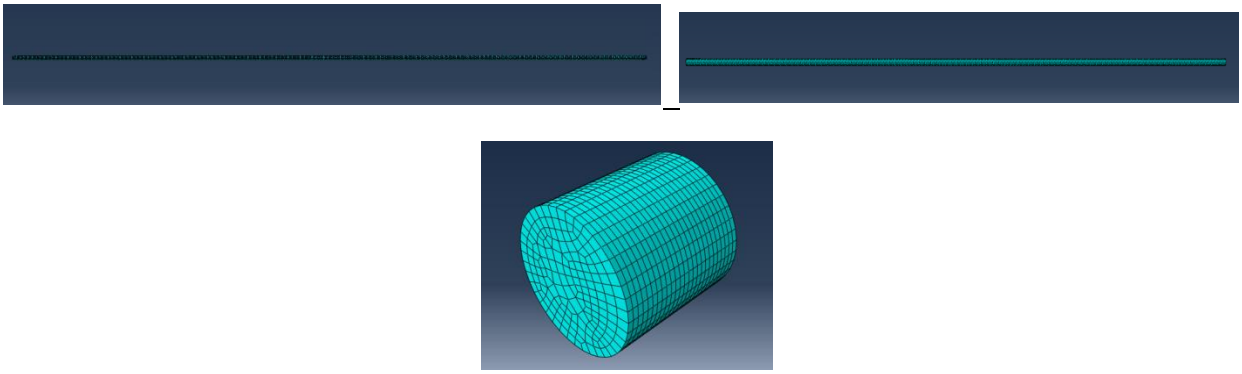

Figure 23: Meshing in the incident bar, transmit bar and sample

Assembling of the bars:

- The bars and the sample are placed in the same line. The sample is placed in between the incident bar and transmit bar as shown in Fig. 24.

Figure 24: The assembled parts of the SHPB setup: the incident bar, sample and the transmit bar

Step definition:

- A Dynamic, Explicit step is defined which uses a central difference scheme to integrate the equation of motion explicitly through time. For a stable condition the time increments (Δt) should be smaller than Courant time limit, $\Delta t < l/c$, where l is length of smallest element and c is the sound wave velocity in medium in which it travels.
- Also, the artificial bulk viscosity for quadratic and linear functions of volumetric strain rates is taken 1.2 and 0.06, respectively.

Interactions between the bar and specimen:

- The interaction property between the incident bar, sample and transmission bar are defined as hard and frictionless.
- The contact between the bar and sample is general contact algorithm.

Boundary conditions:

- The end of the transmission bar is kept fixed as shown in Fig. 25. The boundary conditions are applied to bars and sample such that one-dimensional propagation of wave is allowed. The uniaxial simulations are performed for three different rock types.

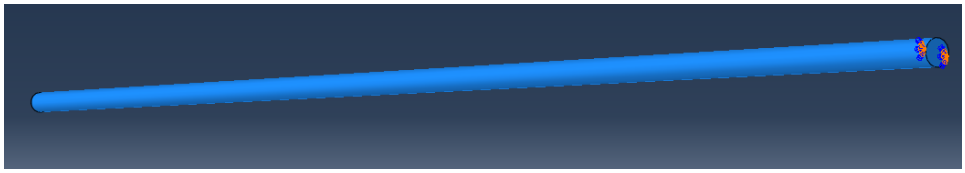

Figure 25: The end of the transmit bar was fixed

Impact load on the incident bar:

- The striker was given a velocity of 8.05m/sec. In SHPB test, when the striker impacts the incident bar in the axial direction, a rectangular stress pulse generates, which propagates along the incident bar. As the length of striker is short as compared to the

total length of the incident bar and the transmission bar, the peak trapezoidal incident stress and the duration of the stress pulse is given by equation (26) and (27).

- The incident stress is applied to the cross-sectional area of the incident bar in a tabular form with maximum stress 162MPa for a time period of 6e-5 seconds is mentioned in Fig. 26.

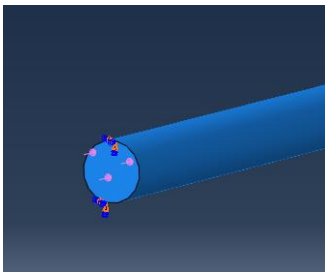

	Time/Frequency	Amplitude
1	0	0
2	1E-006	162000000
3	6E-005	162000000
4	6.1E-005	0

Figure 26: Applied load on the c/s of incident bar and its time variation

Creating Sets to view Output:

- Sets of elements are chosen from the incident bar, transmit bar and sample to view its incident and reflected stress-strain, transmitted stress-strain along with the axial stress strain of the sample.
- For getting the stresses, the stress in the z-direction is chosen while for true strain, logarithm strain is chosen.

Running a job:

- Finally a job is created and submitted to view the results of the SHPB setup modelled.

4.2.2. Modelling and Simulating concrete like material-mortar

The simulation of mortar is same as above except the plasticity model considered here is Drucker-Prager. For analysing the dynamic response of mortar, a 3D model is setup.

Modelling the parts and their properties

- Both the pressure bars – incident and transmit bar are taken as steel and are of same dimensions. The l/*d* ratio for the specimen is taken as 0.5. The properties of the materials are given in the Table 5 taken from the research of Li and Meng (2003).

Table 5: Properties of materials along with its dimensions for SHPB test

	Diameter (mm)	Length (m)	Mass Density, ρ (kg/m^3)	Modulus of elasticity, E (GPa)	Poisson Ratio, ν
Pressure bar (Steel)	20	1	7800	200	0.3
Specimen (Mortar)	12	0.006	2000	2	0.2

- The real value of friction angle of the material for mortar ranges from 40–60°, and therefore, 50° is considered for the numerical simulation in the present study.
- Dilation angle = friction angle of the material, is used in the following simulations.
- They also showed that the characteristic behaviour of mortar specimen is insensitive to K, i.e., flow stress ratio, and thus K=1 is used in this work.
- Fig. 27 indicates the uniaxial quasi-static stress–strain curve of mortar which is simplified from Maher and Darwin (1980). The quasi-static stress–strain relation of the mortar is simplified into a linear elastic relation whose ultimate compressive strength is 40 MPa and ultimate strain is 0.2%, which is trailed by a strain softening region.

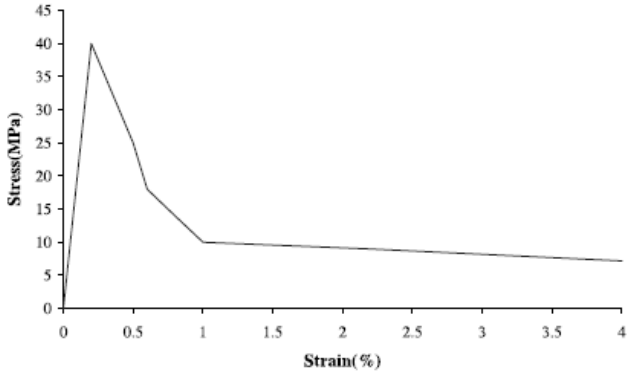

Figure 27: Quasi-static uniaxial stress–strain curve of mortar (Li and Meng , 2003**).**

- Strain-rate sensitivity was implemented by using the quasi-static flow stress and DIF obtained from standard SHPB test for mortar (Grote et al., 2001) shown in Fig. 28.
- The dynamic increase factor (DIF) is an important parameter for measuring the strain-rate effect on the strength of cement mortar.

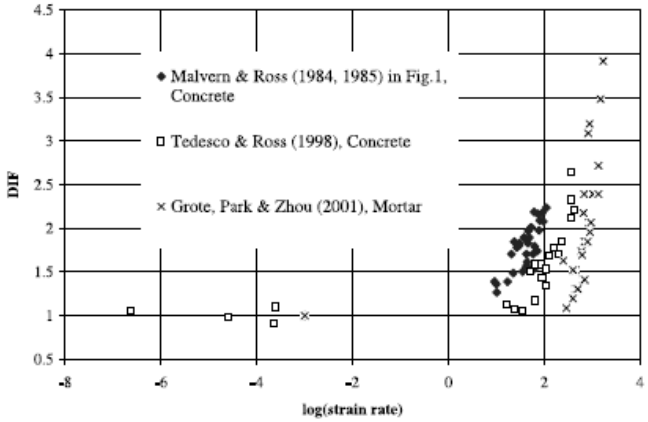

Figure 28: Strain-rate influence on DIF measured by SHPB (Li and Meng , 2003).

Creating Mesh:

- Three dimensional (3D) solid eight node brick elements with reduced integration and hourglass control (C3D8R) are used for meshing the incident bar, transmission bar and the mortar sample.

- The specimen is meshed into 30 elements in the longitudinal direction and 30 elements in radial direction where the pressure bars are divided by 10 elements in radial direction and 800 elements in the longitudinal direction. Finer meshes are done near the bar/specimen interfaces shown in Fig. 29.

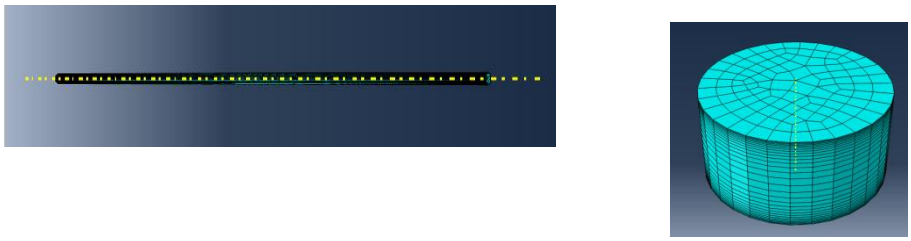

Figure 29: Meshing in pressure bar and sample

Impact load on the incident bar:

- Instead of modelling the striking between a striker bar and the incident pressure bar, a trapezium shaped stress pulse is produced into the incident pressure bar. The rising time of the wave which is tabulated varies from 0 to 180μs while pulse duration varies from 30 to 240μs. Also, the stress intensity is varied from 45 to 1000 MPa to get the desired strain rate for measuring ultimate stress of the SHPB test.

Assembling the parts, defining the steps, assigning interaction properties and giving boundary conditions are the same as that in the rocks that is mentioned in the section 4.2.1.

4.2.3. Modelling and Simulating concrete

The simulation of concrete is first done using only elastic properties and then the deviation is checked by considering its plastic properties. For analysing the dynamic response of concrete, a 3D model is setup and the plasticity model used is Concrete Damaged plasticity model.

Modelling the parts and their properties

- The incident, transmitted and striker bar are taken as steel and the sample is Normal strength concrete of M30. The properties of the materials are given in Table 6.

Table 6: Properties of bars and specimen

Bars	Diameter (mm)	Length (m)	Mass Density, ρ (kg/m^3)	Modulus of elasticity, E (GPa)	Poisson Ratio, ν
Striker bar	60	1	7850	200	0.3
Incident bar	60	4.5	7850	200	0.3
Transmit bar	60	4.5	7850	200	0.3
Specimen	36	0.036	2500	30	0.2

Creating Mesh:

- Three dimensional (3D) solid eight node brick elements with reduced integration and hourglass control (C3D8R) are used for meshing the incident bar, transmission bar and the concrete sample.
- The global size of input and output bar is 0.0085 while that of specimen is 0.0051.

Impact load on the incident bar:

- For getting the strain rate as $350s^{-1}$, 500 s^{-1} and 700 s^{-1}, the velocity of the striker bar to collide with the incident bar are 12.6, 18.0 and 25.2m/sec respectively. Using the equation (26) and (27) the amplitude of stresses for the strain rates 350, 500 and 700 sec^{-1} are 250 MPa, 356 MPa, 500 MPa respectively for the time period of 4e-4 seconds.

Assembling the parts, defining the steps, assigning interaction properties and giving boundary conditions are the same as that in the rocks that is mentioned in the section 4.2.1.

Considering plasticity model, we take the following properties for M30 grade concrete using the equations from (34) to (36).

- Dilation angle is taken as 36.31 while the tensile behaviour is taken from the graphs given in Fig. 30.

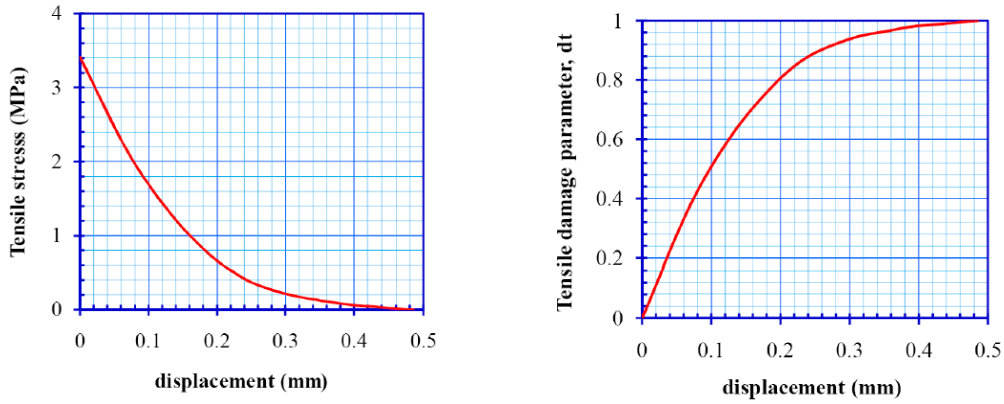

Figure 30: Post failure stiffness degradation damage properties of concrete (a) Stress-displacement relation (b) Tension damage model (Ahmad, 2014)

Rest all methods for analysing the dynamic response of concrete using the plastic properties are the same.

Chapter -5

Results and Discussions

5.1. INTRODUCTION

As explained in the previous chapters following four problem is solved using SHPB model: SIMULINK is very simple programming tool that can be used to model SHPB. Therefore, a problem is taken from literature Yongjian et al. (2010) and solved using SIMULINK to understand the concept of wave propagation to generate stress-strain relation. SIMULINK is found to work well to evaluate stress-strain relation with high strain rate with linear elastic behaviour. The results obtained from SIMULINK are in good agreement with the results presented in the literature (Yongjian et al., 2010). However, we could not use SIMULINK successfully to evaluate nonlinear stress strain relation.

To study the nonlinear stress-strain relation of realistic materials ABAQUS is used for further analysis. Three different materials have been considered for the present study (i) Rock (Granite, Lime Stone and Sand Stone), (ii) Cement Mortar and (iii) Concrete. This section presents the results of all the above four problems and the discussions on the results.

5.2. PROBLEM FROM LITERATURE Yongjian et al. (2010) SOLVED USING SIMULINK

This problem is taken from Yongjian et al. (2010). The details of this problem and the properties of incident bar, transmission bar and the specimen are given in Section 4.1.1. Linear stress-strain relation is derived using three different type of incident waves: (i) Rectangular, (ii) Finite rising and (ii) sloping. Following section presents the results obtained from these three type of incident waves.

5.2.1. Rectangular Incident Wave

Rectangular incident wave (expressed here in terms of stress) is constant with time with finite time period. Incident stress is considered from the Yongjian et al. (2010) as 5E07 Pa for a time period of 3E-05 second as shown in Fig. 31. The Transmitted wave, reflected wave, all the three

waves, strain in the specimen and the stress strain response for rectangular incident wave is shown Figs. 32- 36.

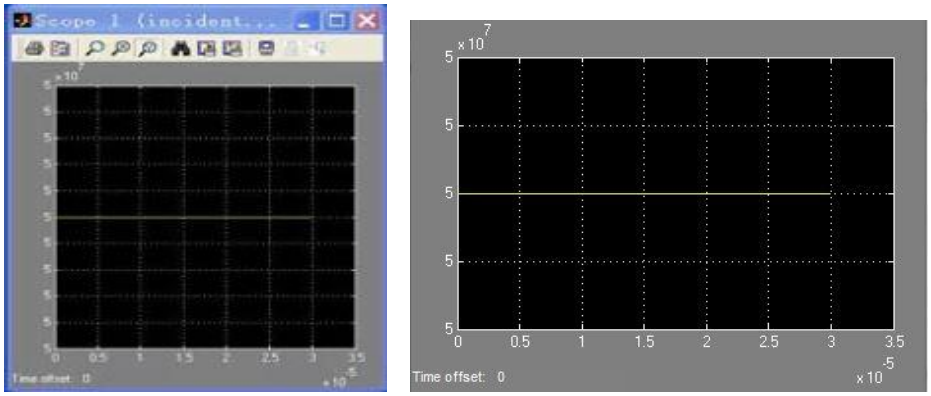

Figure 31: Incident wave in (a) original model (b) present study (rectangular)

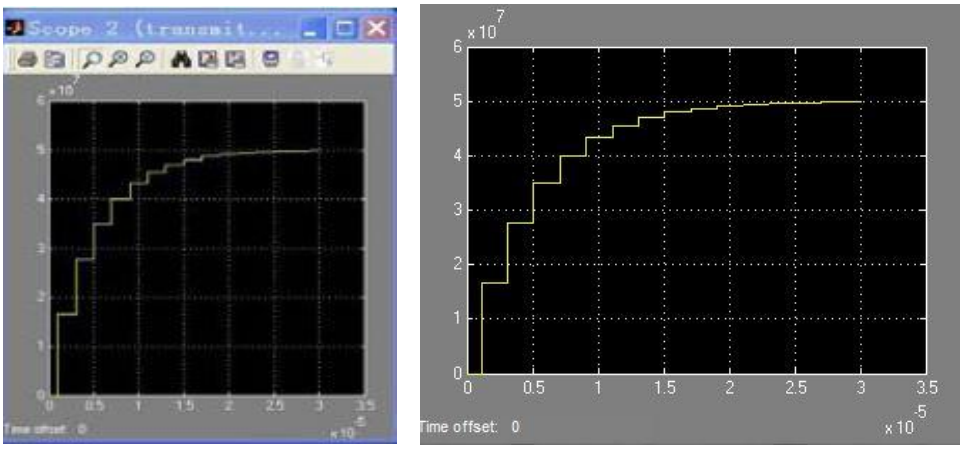

Figure 32: Transmitted wave in (a) original model (b) present study (rectangular)

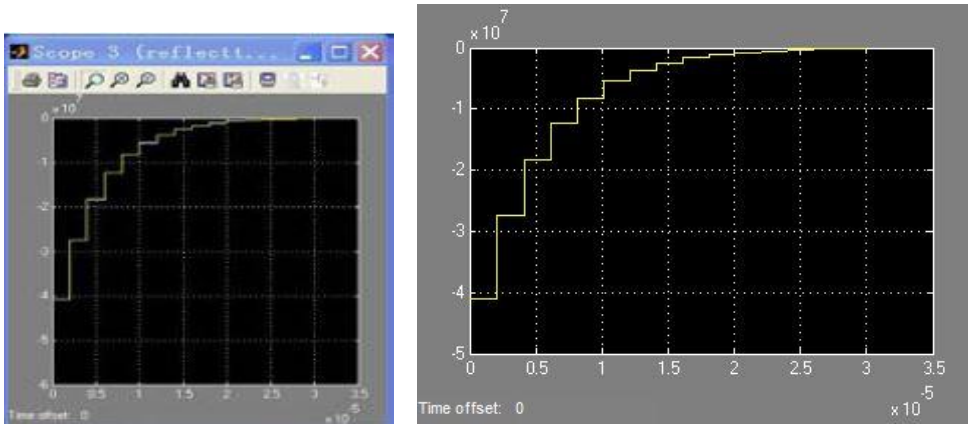

Figure 33: Reflected wave of (a) original model (b) present study (rectangular)

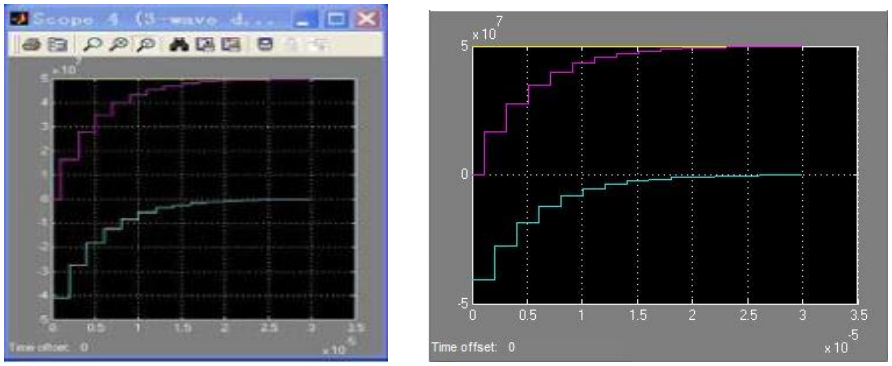

Figure 34: All three waves of (a) original model (b) present study (rectangular)

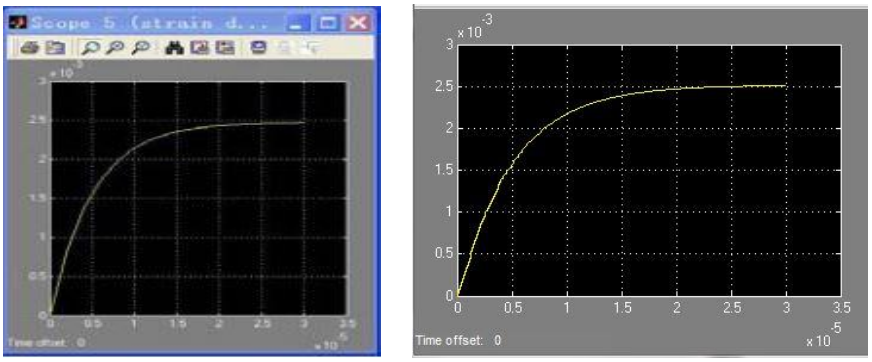

Figure 35: Strain in (a) original model (b) present study (rectangular)

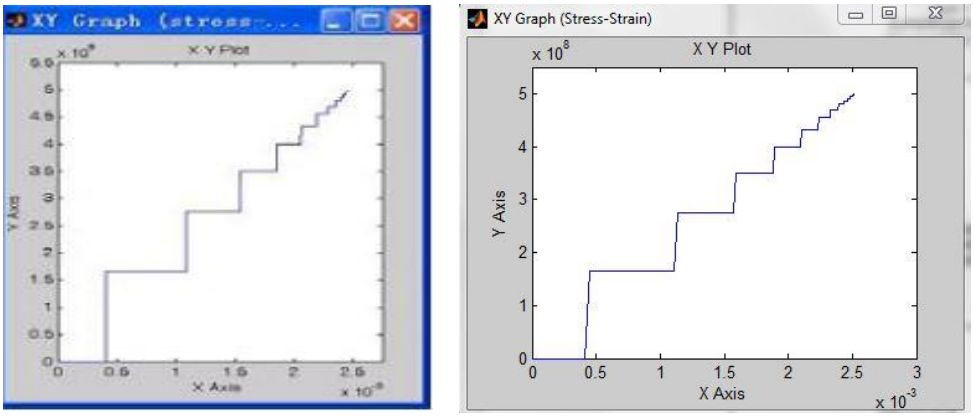

Figure 36: Reconstructed Stress-Strain graph in (a) original model (b) present study (rectangular)

5.2.2. Finite Rising Incident Wave

Finite rising incident wave initially begins from zero, which rises to a particular stress within a short time and becomes constant with time for a finite time period. Incident stress is considered

from the Yongjian et al. (2010) which rises from zero to 5E07 Pa in 2E-06 seconds for a time period of 3E-05 s as shown in Fig. 37. The Transmitted wave, reflected wave, all the three waves, strain in the specimen and the stress strain response for finite rising incident wave is shown Fig. 38- 42.

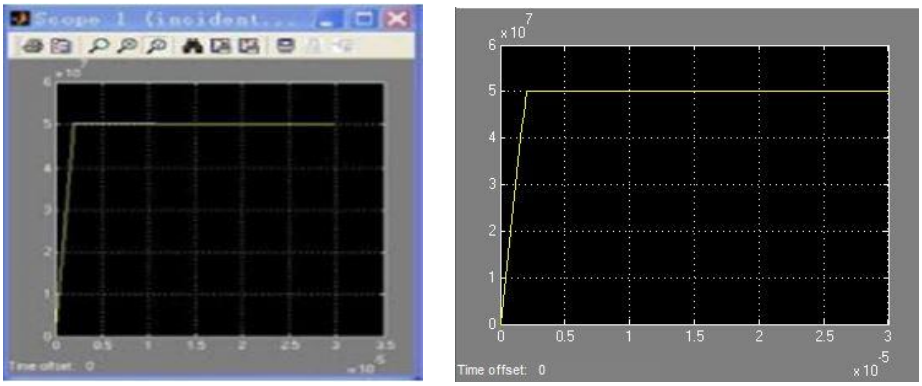

Figure 37: Incident wave in (a) original model (b) present study (finite rising)

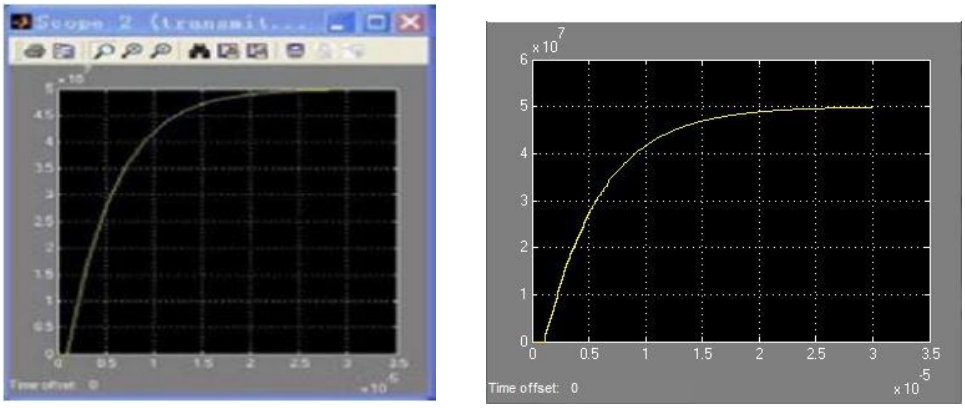

Figure 38: Transmitted wave in (a) original model (b) present study (finite rising)

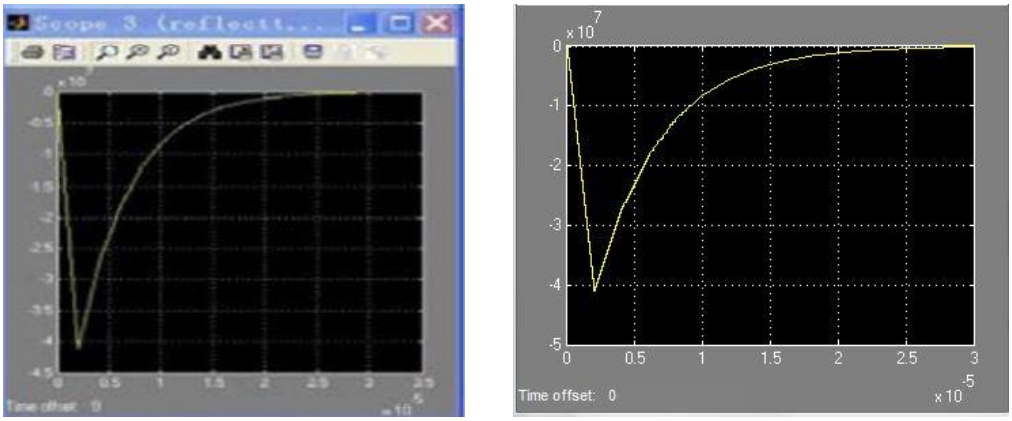

Figure 39: Reflected wave in (a) original model (b) present study (finite rising)

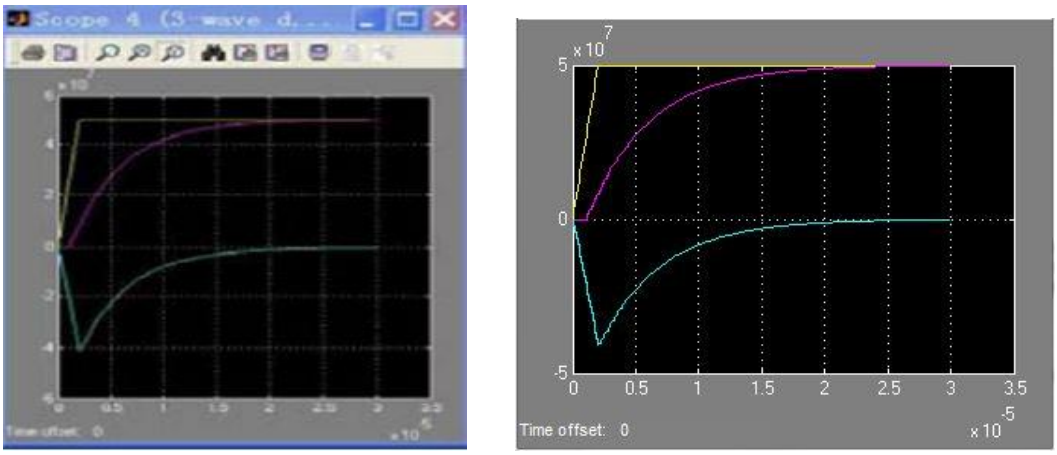

Figure 40: All 3 wave in (a) original model (b) present study (finite rising)

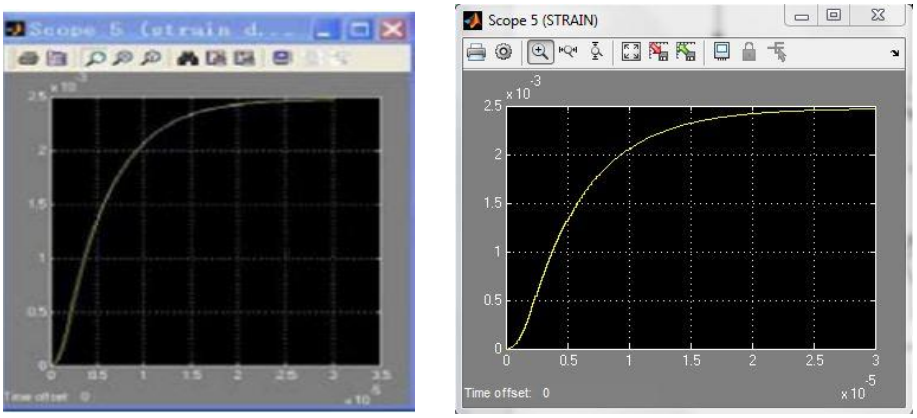

Figure 41: Strain in (a) original model (b) present study (finite rising)

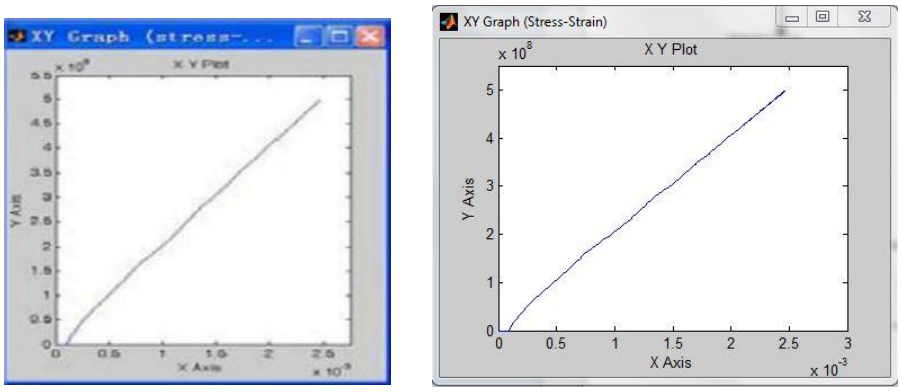

Figure 42: Reconstructed Stress-Strain graph in (a) original model (b) present study (finite rising)

5.2.3. Sloping Incident Wave

Sloping incident wave increases from zero to a particular stress in a finite time period. In Yongjian et al. (2010) incident stress increase from 0 to 5E07 Pa for a time period of 3E-05 seconds as shown in the Fig. 43. The Transmitted wave, reflected wave, all the three waves, strain in the specimen and the stress strain response for finite rising incident wave is shown Fig. 44- 48.

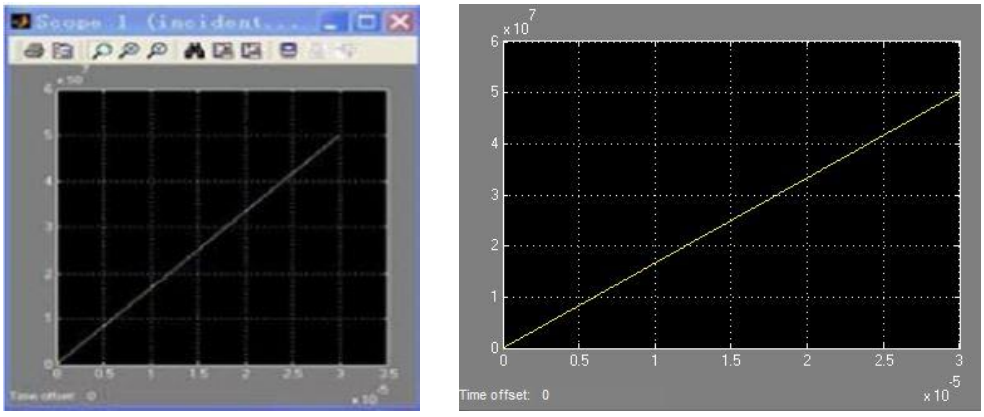

Figure 43: Incident wave in (a) original model (b) present study (sloping)

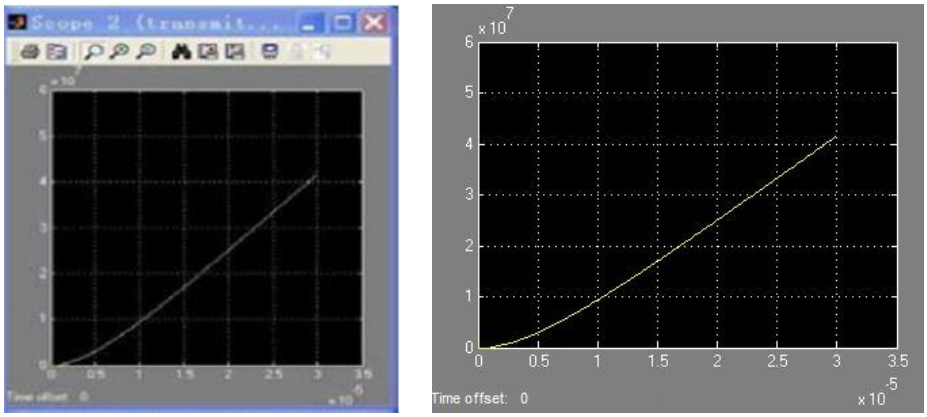

Figure 44: Transmitted wave in (a) original model (b) present study (sloping)

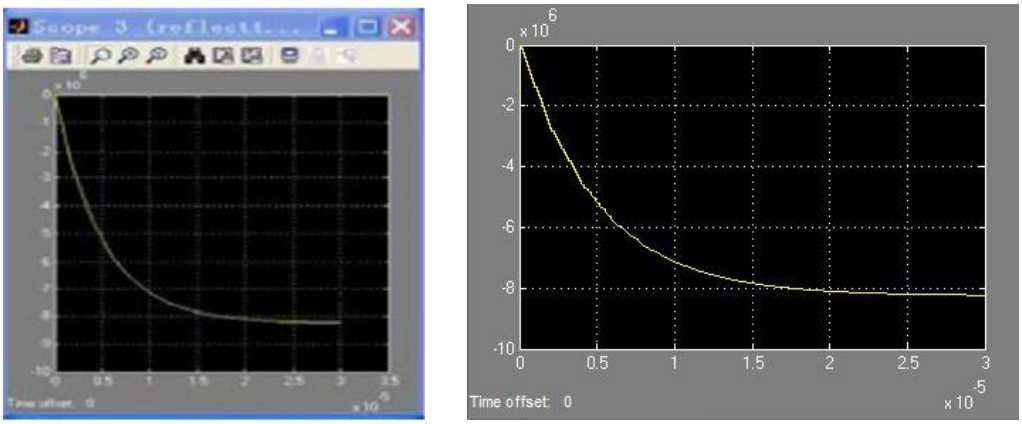

Figure 45: Reflected wave in (a) original model (b) present study (sloping)

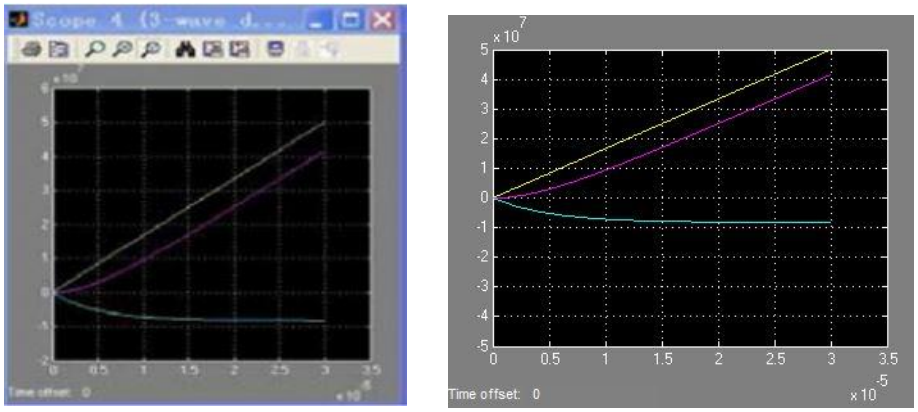

Figure 46: All 3 wave in (a) original model (b) present study (sloping)

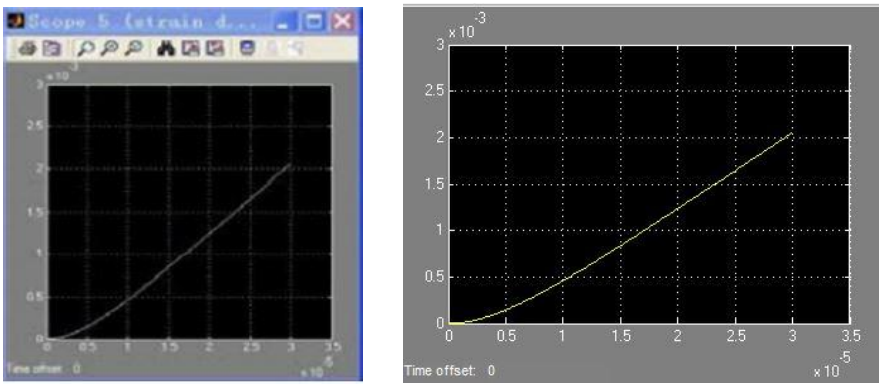

Figure 47: Strain in (a) original model (b) present study (sloping)

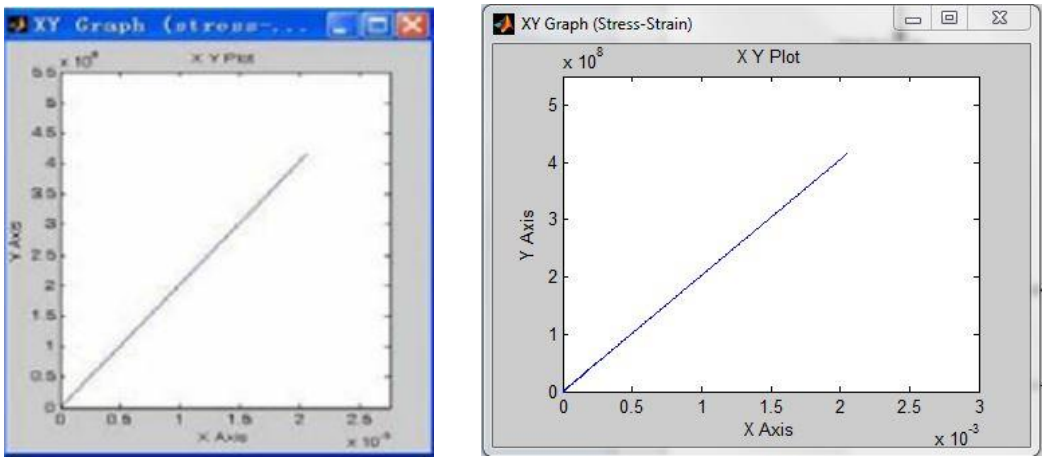

Figure 48: Reconstructed Stress-Strain graph in (a) original model (b) present study (sloping)

5.2.4. Discussions on results of SIMULINK

The above section presents the simulation results for different incident waves. The following features are deduced from the three simulations:

- The modelling process is very convenient, efficient and less time consuming. It takes few seconds to produce the result.
- The models have good visualization. This can produce graph results for both midway and final and are easily understood and operated.
- Many modules can be generated in one model. It can be easily modified for different tasks.

The above three simulations have only considered the simple shaped incident waves. We can obtain the same behaviour if we input an actual incident wave with same signal length. This simulation and its results show that our model has both the theoretical studies along with significant practical values. So it provides gives a decent apparatus for SHPB test design, analysis and its data validation in engineering applications.

5.3. SIMULATION RESULTS OF THE THREE ROCKS DONE USING ABAQUS

The detailed model of SHBP setup in FE software ABAQUS is well explained in section 4.2.1. The axial stress-strain curves of the three materials taken i.e., limestone, weak sandstone and granite are found and are compared with Chakraborty, (2013). Results from the paper are in red and results obtained from the above simulation are in blue.

5.3.1. Limestone

Taking the properties of Limestone and simulating in ABAQUS, the axial stress-strain curve is shown in Fig. 49. The incident and transmitted strain recorded in the bars when limestone is taken as the specimen are shown in Fig. 50.

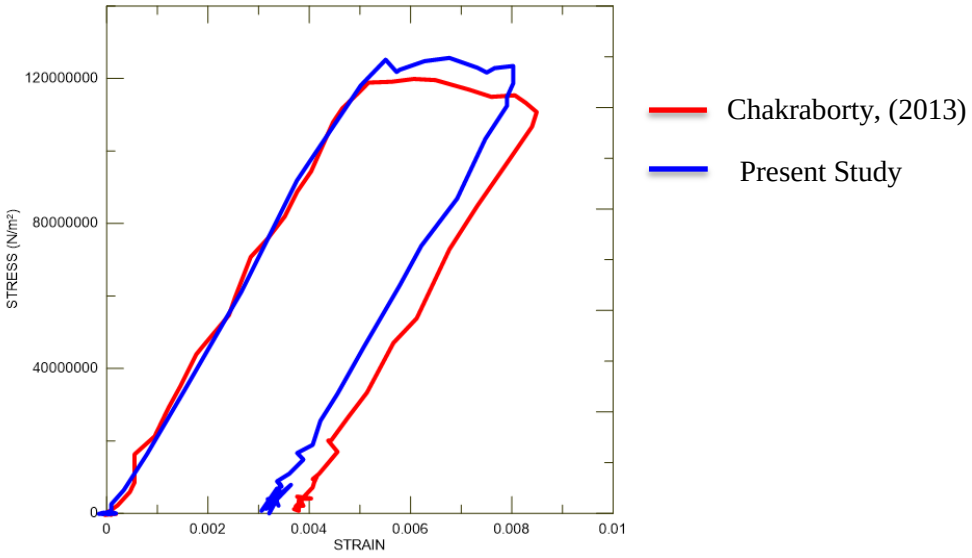

Figure 49: Axial Stress-strain curve for limestone.

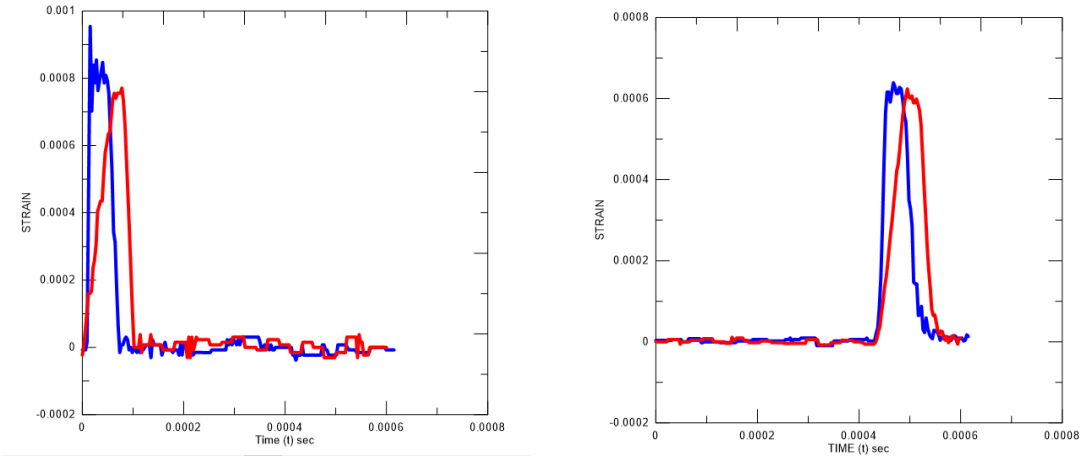

Figure 50: (a) Incident strain in limestone. (b) Transmitted strain in limestone.

5.3.2. Weak Sandstone

Taking the properties of Sandstone and simulating in ABAQUS, the axial stress-strain curve is shown in Fig. 51. The incident and transmitted strain recorded in the bars when sandstone is taken as the specimen are shown in Fig. 52.

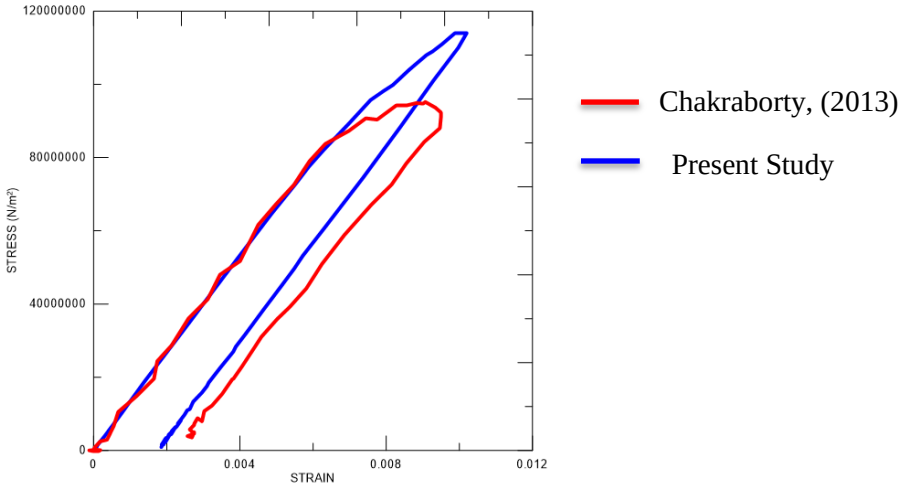

Figure 51: Axial stress-strain curve of sandstone.

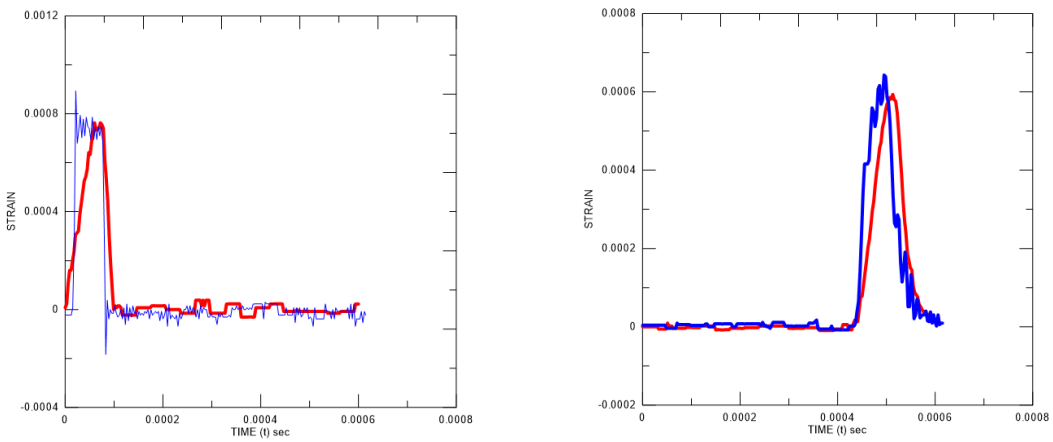

Figure 52: (a) Incident strain in sandstone. (b) Transmitted strain in sandstone.

5.3.3. Granite

Taking the properties of granite and simulating in ABAQUS, the axial stress-strain curve is shown in Fig. 53. The incident and transmitted strain recorded in the bars when granite is taken as the specimen are shown in Fig. 54.

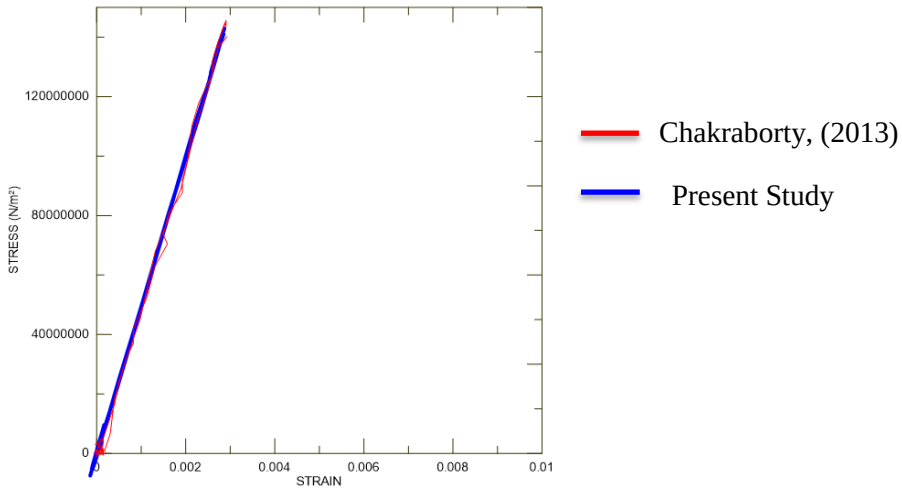

Figure 53: Axial stress-strain curve for granite.

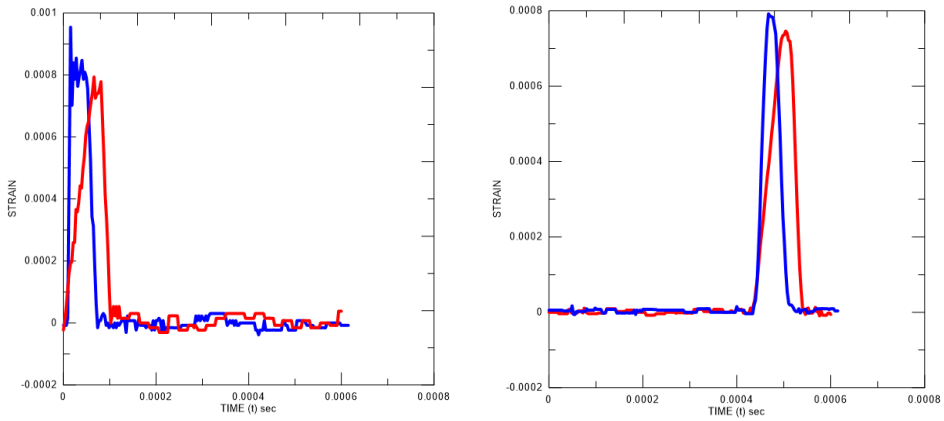

Figure 54: (a) Incident strain in granite. (b) Transmitted strain in granite.

5.3.4. Discussions on results in three rocks

Higher peak stress is observed for rocks with higher stiffness. The initial slope of the stress-strain curves also clearly shows the effect of stiffness of the rocks, i.e. the initial slope decreases with decreasing stiffness of rock. For granite, the loading and unloading paths remain same because granite does not exhibit elasto-plastic response. However, plastic strain is observed in the cases of limestone and weak sandstone which is expected. The incident strains are observed to be same in all the three rocks. However, the transmitted strains are different for the three different rocks. The highest amount of transmitted strain is observed in granite whereas the lowest amount of transmitted strain is observed in sandstone. Higher amount of strain in the transmission bar in the case of granite is due to elastic behaviour of granite in SHPB test and thus the absence of plastic dissipation. Plastic dissipation is present in the cases of limestone and sandstone which results in lower amount of strain transmission in these rocks.

5.3.5. Comparison of Simulation in ABAQUS and SIMULINK

Since analysing the plastic properties of rocks in SIMULINK was not successful, we assumed the rocks to be completely elastic and the three rocks were simulated using both ABAQUS and SIMULINK. The results of the three curves were compared.

Limestone

Since the yield stress of limestone is 68MPa, a stress incident wave of 60MPa at lower strain rate is taken and simulated in all the three setups. Also limestone is considered elastic so its crushable foam property is not considered. The axial stress-strain curves of both the simulation is shown in Fig. 55.

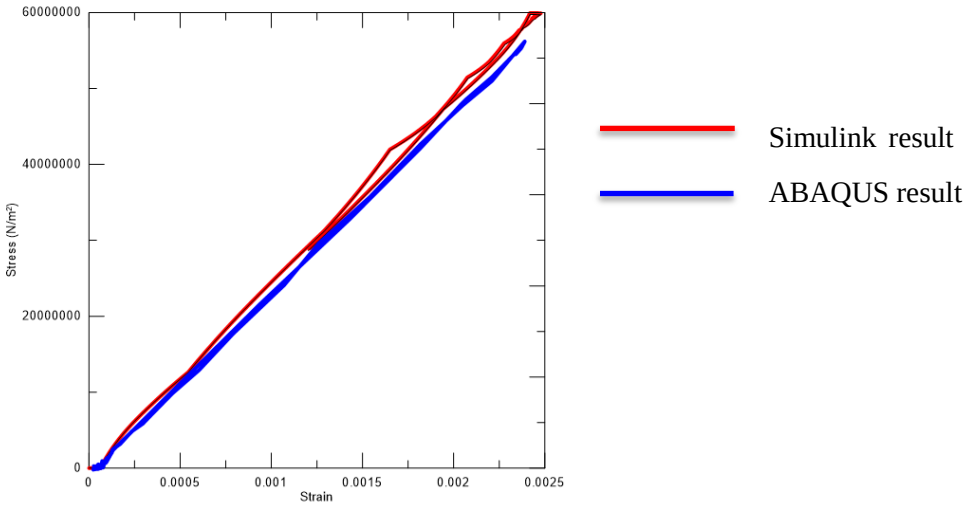

Figure 55: The stress-strain curve of limestone using ABAQUS (blue), MATLAB SIMULINK (red)

Sandstone

Since the yield stress of sandstone is 23MPa, a stress incident wave of 20MPa at lower strain rate is taken and simulated in all the three setups. Also sandstone is considered elastic so its crushable foam property is not considered. The axial stress-strain curves of both the simulation is shown in Fig. 56.

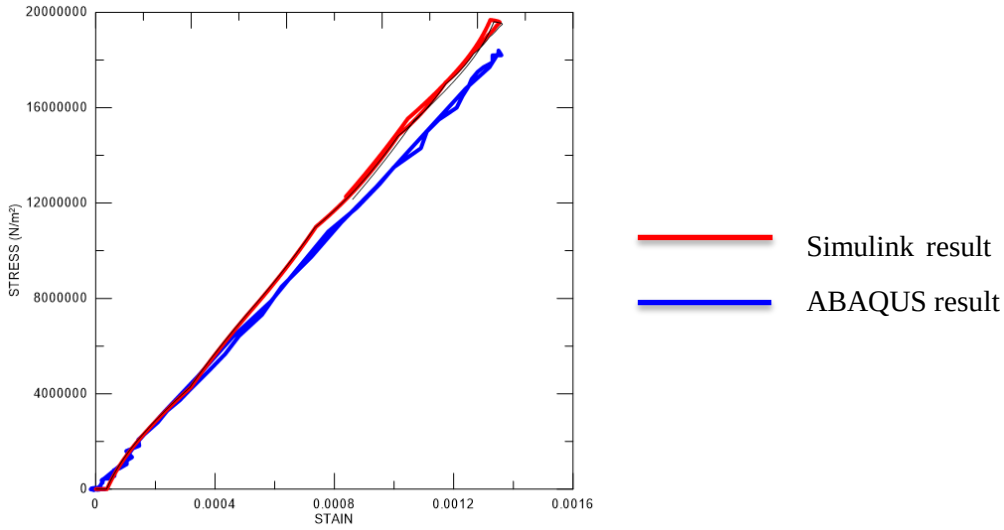

Figure 56: The stress-strain curve of sandstone using ABAQUS (blue), MATLAB SIMULINK (red).

Granite

Since the yield stress of granite is 200MPa, a stress incident wave of 162MPa is taken at lower strain rate and simulated in all the three setups. Granite is considered elastic so its crushable foam property is not considered. The axial stress-strain curves of both the simulation is shown in Fig. 57.

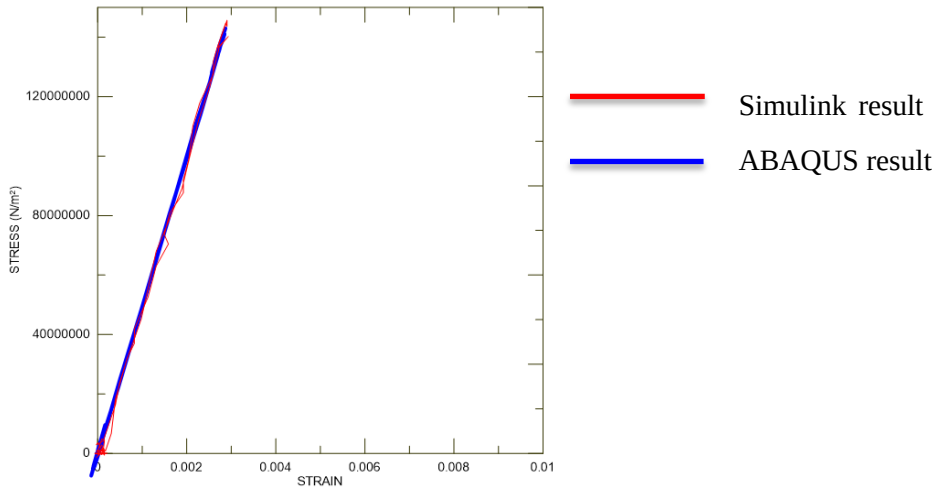

Figure 57: The stress-strain curve of granite using ABAQUS (blue), MATLAB SIMULINK (red).

5.3.6. Discussions on results of comparison

The briefest time to accomplish consistency of stress in a specimen needs the incident pulse to have a particular profile. In SHPB testing, a fundamental presumption is that the stress in the specimen is considered uniform during the test. This supposition may not hold good when the specimen is excessively fragile, on the grounds that the specimen collapse during initial loading before attaining the equilibrium of stress, especially when the velocity of wave in the specimen is very slow.

5.4. SIMULATION RESULTS OF CEMENT MORTAR

The detailed model of SHBP setup for cement mortar in FE software ABAQUS is well explained in section 4.2.2. The axial stress-strain curves of mortar is found and compared with Li and Meng (2003). The analysis by Li and Meng (2003) was done taking two dimensional models while in the present study three dimensional models were considered. Results from the paper are in red and results obtained from the above simulation are in blue. The axial and hydrostatic stress versus the axial strain at nominal strain rate of 27 s^{-1} is shown in Fig. 58 and at nominal strain rate of 390 s^{-1} is shown in Fig. 59. Here the stresses are in N/m^2.

Li and Meng (2003)

Present Study

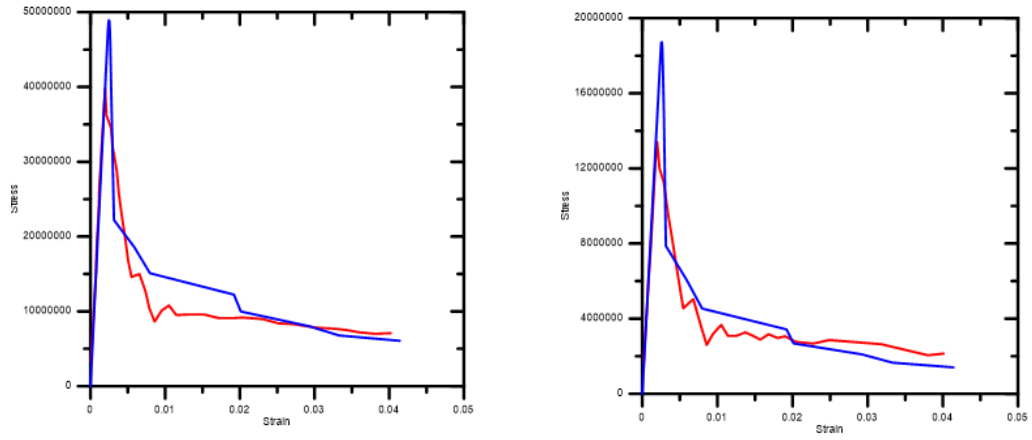

Figure 58: (a) The axial stress-strain at a nominal strain-rate of $27s^{-1}$ (b) The hydrostatic stress-strain at a nominal strain-rate of $27s^{-1}$.

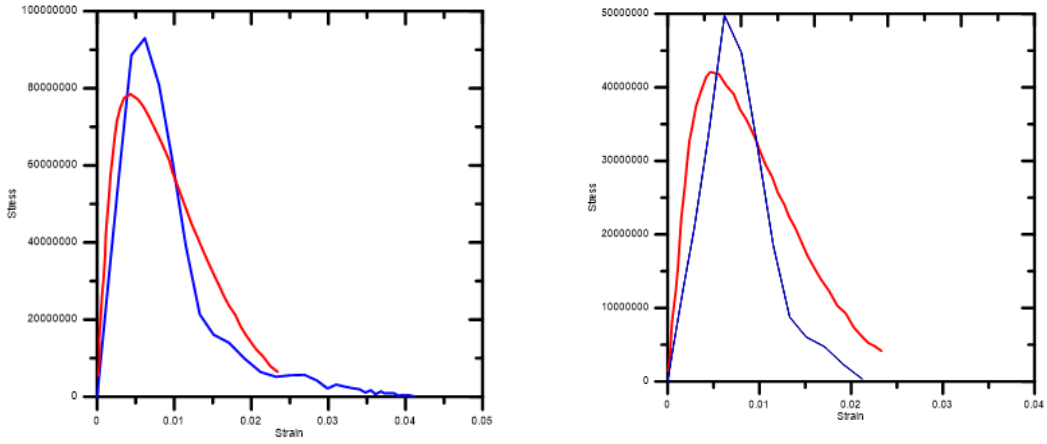

Figure 59: (a) The axial stress-strain at a nominal strain-rate of $390s^{-1}$ (b) The hydrostatic stress-strain at a nominal strain-rate of $390s^{-1}$

5.4.1. Observations in results of mortar

- It is observed that at the nominal strain-rate of $27s^{-1}$ the stress–strain curve almost fits the input quasi-static uniaxial stress strain curve, especially before it reaches the ultimate compressive strength. There is no effect of strain rate on the hydrostatic stress which comes out to be almost one-third of the uniaxial compressive stress.

- It implies that other two principal stresses σ_1 and σ_2 are 0 at that nominal strain-rate ($27s^{-1}$) and the stress state in larger part of the sample material is uniaxial in this numerical SHPB test.
- However, by increasing the strain-rate, both the Young's modulus and the ultimate strength increase extensively. The ultimate compressive strength which is measured is almost twice of its quasi-static value.
- The average hydrostatic stress in the specimen is a little more than half of the compressive stress, which means that other two principal stresses are non-zero, i.e., $\sigma_1 = \sigma_2 \neq 0$.

5.3.2. Discussions on results of mortar

- There is a deviation in this ''reconstituted'' axial stress–strain relation from the quasi-static axial stress–strain relation which is due to the violation of the fundamental considerations in a SHPB test.
- The numerical simulations of SHPB tests done considering a low strain-rate, the hydrostatic stress of the tested specimens is uniform. Also, the lateral confinement due to the lateral inertia is immaterial.
- In the numerical SHPB tests there are no apparent strain-rate effects for the current material model observed at lower strain rates.
- But at high strain rates due to lateral confinement lateral inertia comes to play in the specimen, as it restricts the radial expansion of the specimen causing lateral confinement.

5.5. SIMULATION RESULTS OF CONCRETE

The three dimensional elastic model of NSC is studied and analysed based on the finite element method. Since the present model with elastic properties of concrete was unable to completely satisfy the experimental results conducted by Hentz et al. (2004) so, the analysis was performed considering the plastic behaviour of concrete.

With the elastic properties the model is simulated and the stress strain behaviour of concrete under uniaxial compression with different strain rate of $350s^{-1}$, $500s^{-1}$ and $700s^{-1}$ are shown in Fig. 60. According the experimental results by Hentz et al. (2004), the peak stresses at strain rate of $350s^{-1}$, $500s^{-1}$ and $700s^{-1}$ are 57.5MPa, 75MPa and 104MPa. After considering the plasticity model, stress strain behaviour of concrete with different strain rate of $350s^{-1}$, $500s^{-1}$ and $700s^{-1}$ are shown in Fig. 61 along with static stress-strain behaviour from Babu and Rao (2014).

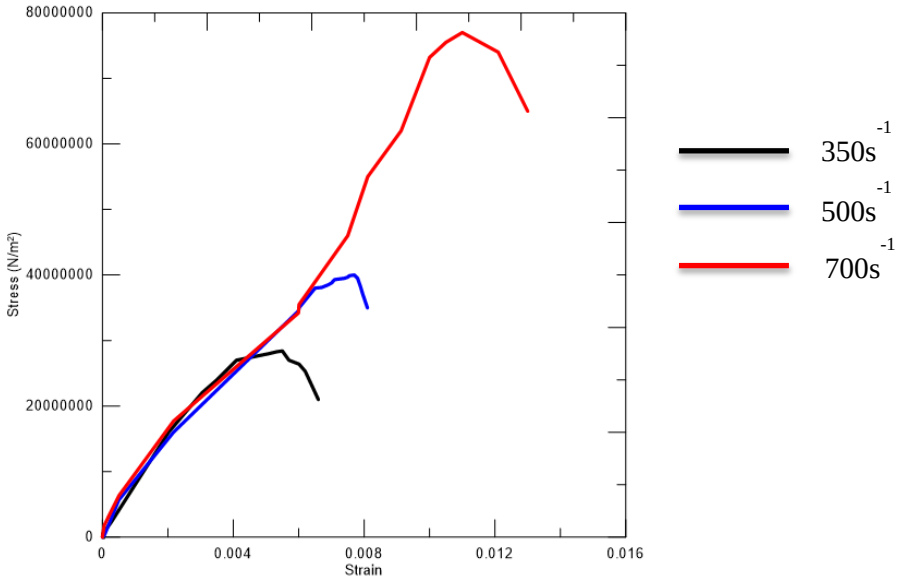

Figure 60: Stress strain behaviour of concrete with different strain rate of $350s^{-1}$ (black), $500s^{-1}$ (blue) and $700s^{-1}$ (red) considering the elastic properties only

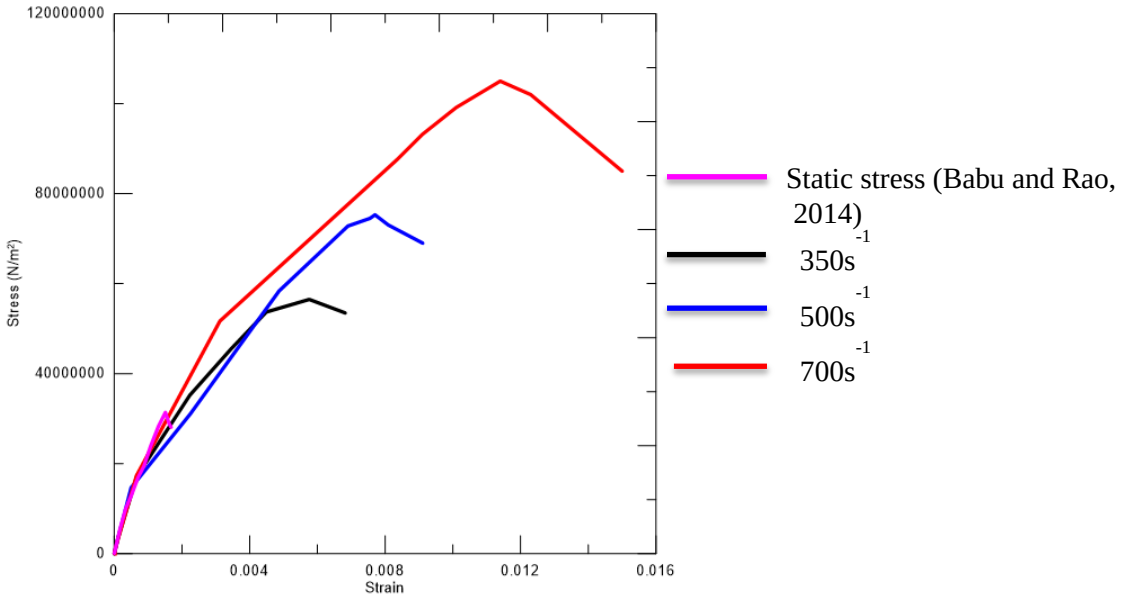

Figure 61: Stress strain behaviour of concrete with different strain rate of $350s^{-1}$(black), $500s^{-1}$ (blue) and $700s^{-1}$ (red) considering the plastic properties along with static stress strain from (Babu and Rao, 2014) (magenta)

5.5.1. Discussions of results of concrete

- The peak stresses of cylindrical NSC specimens with only elastic properties are 28.4, 40.0 and 77.0 MPa while the strains at its maximum are 0.0067, 0.0083 and 0.0142, respectively.
- The peak stresses of cylindrical NSC specimens considering the plastic properties are 56.5, 75.3 and 105.0 MPa while the strains at its maximum are 0.0068, 0.00911 and 0.015, respectively.
- The comparative study shows +98.94, +88.25 and +36.36% deviation from the numerical results due to only elastic properties to results considering the plastic properties of concrete at the strain rate of 350, 500 and 700 sec^{-1}, respectively. The dynamic properties of NSC are affected by elasticity, strain rate and rapidly changed to plastic from elastic state at time of failure.

Chapter -6

Summary and Conclusion

6.1. SUMMARY

The analysis of structure subjected to blast loading requires constitutive (stress-strain) relation under high strain rate. There are many literature present the constitutive relation of different civil engineering materials including concrete under high strain rate. Some of these results are based on SHPB experiments and others are based on computer simulation. A detailed literature review reveals that although there are many experiments conducted on concrete in USA and Europe in this regard there are no study reported on the nonlinear stress-strain behaviour using computer simulation. Therefore, the main objective of the present study is identified as to evaluate the nonlinear stress-strain behaviour of cement mortar and concrete under high strain rate through computer simulation using SIMULINK and ABAQUS.

To achieve this objective wave propagation in SHPB and associated formulation is studied. The experimental set-up for SHPB is modelled using the toolbox in SIMULINK. A problem is taken from literature (Yongjian et al., 2010) to evaluate linear elastic stress-strain behaviour of a hypothetical material under high strain rate and solved using the SHPB model made in SIMULINK. The results of this analysis found to be in good agreement with the results given in Yongjian et al. (2010).

A second problem is taken from literature to evaluate the nonlinear stress-strain relation of realistic materials (three different type of rocks) and solved using the model generated in SIMULINK. The results shows that SIMULINK can successfully predict the linear elastic behaviour. However, it is found to be not suitable for predicting the nonlinear behaviour of materials under high strain rate.

The same problem then modelled again using finite element software ABAQUS. And the result shows that ABAQUS can accurately predict both linear and nonlinear stress-strain response of

material with high strain rate. This is because ABAQUS which has in-built plasticity models. The plastic properties of materials are found and used as inputs which the software processes to give the desired results. The programming tool SIMULINK doesn't have such models so the formulations of wave propagations are to be generated using the blocks

The most important materials used for constructing structures are concrete. In the regions where blast resistant structures are required, the dynamic responses of concrete are to be found at high strain rates. Since the effectiveness of the experimental setup in ABAQUS is validated using the three different types of rocks, the same model can be used for simulating concrete by acquiring their plastic properties. Therefore concrete and cement mortar is studied using ABAQUS. The properties of cement mortar and concrete are found and stress strain responses of both the materials with different strain rates are obtained.

For cement mortar, the axial stress-strain of nominal strain rate of 27 s^{-1} and 390s^{-1} evaluated whereas the behaviour of concrete is studied under three different strain rates (350 s^{-1}, 500s^{-1} and 700 s^{-1})

6.2. CONCLUSIONS

The salient conclusions of the present study are as follows:

i) SHPB is a very useful method to evaluate the dynamic stress-strain relation under high strain rate

ii) SIMULINK is effective and user friendly tool to simulate the SHPB experiment and develop linear elastic stress-strain relation under high strain rate. However, this tool fails to simulate nonlinear dynamic material behaviour.

iii) ABAQUS is found to yield both linear and nonlinear dynamic stress-strain relation using the SHPB model accurately as it has in-built plasticity models.

iv) The dynamic nonlinear stress strain behaviour under low strain rate does not show significant increase in peak stress (with respect to quasi-static stress) for both cement mortar (at $27s^{-1}$) and concrete (Babu and Rao, 2014). However, at high strain rate the peak stress increases significantly for both the materials considered. At $390s^{-1}$ the cement mortar shows 93.87% increase in peak stress over its quasi-static value. Similarly, at $700s^{-1}$ the concrete shows 236.5% increase in peak stress over its quasi-static value.

6.3. FUTURE SCOPE OF WORK

Although the SIMULINK is easiest and most user friendly programming tool, the samples which have elastic properties only are analysed in the SIMULINK in the present study. This study can be extended by analysing the non-linear materials using SIMULINK. This can be done by formulating the relevant plasticity models in this programming tool.

REFRENCES

1. SIMULINK User's Guide the MathWorks, Inc., 2012. Version R2012B
2. ABAQUS v6.11 user's manual (2011), ABAQUS Inc., DS Simulia, Providence, RI, USA.
3. Yongjian M. et al. (2010), A MATLAB/SIMULINK-based method for modeling and simulation of split Hopkinson bar test, World Journal of Modelling and Simulation-Vol. 6 No. 3, pp. 205-213.
4. Frew D.J. et al. (2005), Pulse Shaping Techniques for Testing Elastic-plastic Materials with a Split Hopkinson Pressure Bar, Society for Experimental Mechanics- Vol 45, No. 2.
5. Song B., Chen W. (2004), Dynamic Stress Equilibration in Split Hopkinson Pressure Bar Tests on Soft Materials, Society for Experimental Mechanics- Vol. 44, No. 3.
6. Goel M.D., Matsagar V.A. (2013), Blast resistant design of structures, Practice Periodical on Structural Design and Construction.
7. Song B., Chen W. (2005), Split Hopkinson pressure bar techniques for characterizing soft materials, Latin American Journal of Solids and Structures-2 113-152.
8. Davies E., Hunter S. (1963), The dynamic compression testing of solids by the method of the Split Hopkinson pressure bar, Journal of the Mechanics and Physics of Solids- 11: 155–179.
9. Yang L., Shim V. (2005), An analysis of stress uniformity in split Hopkinson bar test specimens, International Journal of Impact Engineering-31: 129–150.
10. Hu S. (2005), The application development of experimental technique of Hopkinson pressure bar, Journal of Experimental Mechanics-20: 589–594.
11. Li X.B. et al. (2006), The extended application of Hopkinson bar technique, Explosion and Shock Waves-26:385–394.

12. Chakraborty T. (2013), Impact Simulation of Rocks under SHPB Test, Proc Indian natn Sci Acad -79 No. 3 Spl. Issue, pp.
13. Frew D. J. et al. (2001), A Split Hopkinson Pressure Bar Technique to Determine Compressive Stress-strain Data for Rock Materials, Experimental Mechanics- Vol. 41, No 1.
14. Song B., Chen W.(2004), Dynamic Stress Equilibration in Split Hopkinson Pressure Bar Tests on Soft Materials, Society for Experimental Mechanics- Vol. 44, No. 3.
15. Deshpande V. S., Fleck N. A. (2000), Isotropic constitutive model for metallic foams, J Mech Phys Solids 48, 1253-1276.
16. Li X. B. et al. (2000), Oscillation elimination in the Hopkinson bar apparatus and resultant complete dynamic stress strain curves for rocks, Int J Rock Mech Min Sci- 37(7) 1055-1060.
17. Duba B. et al, (2010), The Brittle-Ductile Transition in Rocks, The Heard Volume:162.
18. Song B., Chen W. (2005), "Split Hopkinson pressure bar techniques for characterizing soft materials" Latin American Journal of Solids and Structures-2 113-152.
19. Nemat-Nasser S. (2000), Introduction to High Strain Rate Testing, Mechanical Testing and Evaluation, Vol 8, ASM Handbook, ASM International, p 427–428.
20. Hopkinson B. (1914), A Method of Measuring the Pressure Produced in the Detonation of High Explosives of by Impact of Bullets, Philosophical Transactions of the Royal Society London. Pg.437-456.
21. Li Q., Meng H. (2003), About the dynamic strength enhancement of concrete-like materials in a split Hopkinson pressure bar test, Int J Solids Struct-40:343–60.
22. Bischoff PH., Perry SH. (1991), Compression behaviour of concrete at high strain-rates, Mater Struct-24:425–50.

23. Grote D.L. et al. (2001), Dynamic behaviour of concrete at high strain-rates and pressures: I. Experimental characterization. Int. J. Impact Engng -25, 869–886.
24. Maher A., Darwin D. (1980), Mortar constitutive of Concrete Under Cyclic Compression, A Report on Research Sponsored by The National Science Foundation Research Grants, ENG 76-09444, CME 79-18414, University of Kansas Lawrence, Kansas.
25. Ahmed A. (2014), Modeling of a reinforced concrete beam subjected to impact vibration using ABAQUS, International Journal of Civil And Structural Engineering, Volume 4, No 3.
26. Hasan et al. (2010), Stress Strain Behavior of Normal Strength Concrete Subjected to High Strain Rate, Asian Journal of Applied Sciences, 3: 145-152.
27. Hinman E. (2011), Blast Safety of the Building Envelope, Whole Building Design Guide, http://www.wbdg.org/resources/env_blast.php, May 21, 2015.
28. Reddy J.N. (2006), An Introduction to the Finite Element Method (Third ed.). McGraw-Hill. ISBN 9780071267618.
29. Hrennikoff A. (1941), Solution of problems of elasticity by the framework method, Journal of applied mechanics **8.4**: 169–175.
30. Courant R. (1943), Variational methods for the solution of problems of equilibrium and vibrations. Bulletin of the American Mathematical Society **49**: 1–23
31. Song B., Chen W., (2011), Split Hopkinson (Kolsky) bar, In Design, testing and applications, New York, Wiley & Sons , pp. 105- 170.
32. Chen W. (2010), Split Hopkinson Bars for Dynamic Structural Testing, p. 183 – 193.
33. Hentz S. et al. (2004), Discrete element modelling of concrete submitted to dynamic loading at high strain rates Computer Structures, 8: 2930.

34. Babu C. V., Rao V.K.V (2014), Behaviour of M30 Grade concrete with confinement under axial compression, International Journal of Engineering Research and Applications, ISSN: 2248-9622, Vol-4, Issue 9(version-5), pp.75-80.